(2)

"Water mass subduction and the transport of phytoplankton in a coastal upwelling system"

Libe Washburn[1], David C. Kadko[2],
Burton H. Jones[1], Thomas Hayward[3],
P. Michael Kosro[2], Timothy P. Stanton[4],
Adriana Huyer[2], Steve Ramp[4], and Timothy Cowles[2]

[1]University of Southern California, Los Angeles, CA
[2]College of Oceanography, Oregon State University, Corvallis, OR
[3]Scripps Institution of Oceanography, La Jolla, CA
[4]Naval Postgraduate School, Monterey, CA

ABSTRACT

Observations during the Coastal Transition Zone (CTZ) experiment in summer, 1988 reveal the presence of deep phytoplankton layers in a coastal upwelling system. The layers occur throughout the CTZ study area, including a strong baroclinic jet which was present over the period of the experiment. Based on a variety of bio-optical, hydrographic, and geochemical indicators, it is concluded that the water masses associated with the layers result from subduction processes. Criteria are developed to identify subducted water masses based on the beam attenuation coefficient, chlorophyll fluorescence, and distribution of light in the water column. Temperature-salinity characteristics are consistent with two source regions for the subducted layers, one near shore and a second farther offshore. Most of the layers correspond to the inshore source which is apparently distributed alongshore. Subducted water masses are found in all 5 grid surveys of the CTZ experiment and probably result from a variety of physical processes. One of these is flow along sloping isopycnal surfaces due to advection and mixing processes. Advection timescales for flow out the axis of jet range from a few days to a few weeks, depending on the depth of a particular surface, and the bio-optical indicators for subduction processes persist over these time scales.

1. INTRODUCTION

An unanticipated observation during the Coastal Transition Zone (CTZ) experiment is the occurrence of layers of high concentrations of phytoplankton at depths often greatly exceeding the euphotic zone. These layers are found both near shore and offshore within a productive coastal upwelling system off northern California and are often observed in a strong offshore jet that was present in the CTZ study area in 1988. We explore the hypothesis that the water masses associated with these layers originate near the surface in the euphotic zone and are subseqently transported downward by vertical circulation processes or subduction (other terms such as subsidence or downwelling are equally descriptive). The subduction hypothesis is supported by a variety of physical, biological, and geochemical indicators including ^{222}Rn, dissolved O_2, and chlorophyll (Kadko et al 1990).

This movement of large volumes of water out of the surface layer (euphotic zone) is potentially important to the vertical transport of heat, mass, salt, and other scalars. Furthermore, geochemical data indicate that this transport can be rapid with vertical velcocities of order 20 -30 m/day (Kadko et al 1990). It also may result in a high vertical flux of organic carbon and represents a mechanism which could quickly remove large concentrations of phytoplankton from the euphotic zone in a productive coastal environment.

At this point, the characteristics of subducted water masses and the mechanisms leading to their subduction in a coastal region are not well understood. Some basic questions include: What are the thicknesses, horizontal extents, and volumes of subducted water masses? Are subducted water masses associated with offshore jets or are they found randomly in the CTZ? Where are the source regions for the subducted water masses? Are the source regions local in the sense that subduction results from vertical sinking with little horizontal advection? Or, is hoizontal advection strong enough to move subducted water masses away from the region where sinking occurs? Are subducted waters transported offshore and, if so, at what rates? What physical processes lead to subduction?

Experimentally, it is necessary to determine quantities and criteria that can be used to establish that an observed water mass has been subducted. It is also important to determine the effective decay times for various subduction indicators.

2. EXPERIMENTAL PROCEDURE

A more complete description of the shipboard observations from the CTZ experiment during the summer, 1988 is presented by Huyer et al (1990). Basically, the overall strategy was to sample a region of the CTZ between Pt. Reyes and Pt. Arena, California over a period of several weeks in order to observe the evolution of strong coastal jets which have been observed previously in the area (cf. Flament et al,

1985 and Davis, 1985). To do this, six hydrographic grid surveys of more or less uniform spatial coverage were made sequentially from three ships: R/V's Wecoma, Pt. Sur, and Thomas Washington (leg 1). (The sampling grids for 5 of these surveys are indicated in Fig. 4.) Due to adverse weather conditions, the entire leg 1 grid survey from the Thomas Washington could not be completed (This incomplete grid is shown in Fig 12). However, the inshore part was completed and is used here to examine nearshore water properties. In addition, during leg 2 of the Thomas Washington survey, sampling was specifically directed at observing physical, biological and chemical distributions in the offshore jet with some limited sampling outside the jet (station locations are indicated by triangles in Fig. 5). The period of this "process sampling" was 18 days (4 July to 21 July) and coincided with the first two hydrographic grid surveys of the Pt. Sur which were conducted from 6 to 18 July.

Measured variables from all vessels include conductivity, temperature, depth (CTD), chlorophyll fluorescence, beam transmission and meteorological observations. Fluorometers and transmissometers were manufactured by Sea-tech, Inc. and each transmissometer has a 0.25 m path length with a 660 nm wavelength light source. Rosettes with Niskin bottles were used in conjuction with the CTD instrumentation to provide bottle sampling for salinity calibration, dissolved O_2, nutrients, chlorophyll, and pigments. Continuous profiles of photosynthetically available radiation (PAR) were made from the Thomas Washington using a sensor manufactured by Biospherical Instruments, Inc.

3. EVIDENCE FOR SUBDUCTION

The primary evidence for subduction processes discussed here is layers of phytoplankton which are observed at depths below the euphotic zone. Because phytoplankton are green plants, they require light for photosynthesis and grow in the illuminated layers of the upper ocean. The presence of phytoplankton in the water column is detected by a combination of chlorophyll fluorescence and beam attenuation coefficient (beam c) profiles. Beam c is a quantitative measure of water column turbidity which depends upon various aspects of the particle field such as particle concentrations, size distribution, and index of refraction (cf. Jerlov, 1976; Baker and Lavelle, 1984). Vertical profiles of beam c and chlorophyll fluorescence at stations containing phytoplankton layers are highly correlated and the presence of phytoplankton in these layers is verified by bottle samples. Such a station located 50 km west of Pt. Arena and in a region of strong southward flow is shown in Fig. 1.

Beam c values exceed 0.4 m^{-1} and the chlorophyll fluorescence signal is above the noise level almost everywhere above 190 db (Fig. 1B). The measured 1% light level here is 31 db and three distinct layers are found: 1) a near surface layer above the 1% light level where chlorophyll concentrations are as high as 8.6 $\mu g/l$, 2) a deeper layer which extends from the 1% light level to about 110 db, and 3) a very deep layer with low beam c and and fluorescence levels

which extends from 125 to 190 db. No surface mixed layer is observed and gradients in all measured quantities extend to the surface. A weak temperature inversion is present on the upper boundary of layer 2 (Fig. 1C) and suggests that this layer is intrusive, a conclusion also supported by the T-S diagram for this station. Examples of several T-S diagrams showing an association between deep fluorescence layers and relatively warm, fresh anomalies are given by Kadko et al (1990).

A very different type of profile is typically found in offshore waters away from the jet, such as at station E-4 (Fig. 1A). A deep fluorescence layer is centered at about 93 db, well below the 60 db deep surface mixed layer, and lies just below the 1% light level at 85 db (Fig. 2A and 2B). Chlorophyll concentrations from bottle samples are about 0.5 $\mu g/l$ just above and below the fluorescence peak, apparently the peak itself was missed in sampling. However, chlorophyll and fluorescence are highly correlated and nearby stations show peak concentrations of about 1 $\mu g/l$. Chlorophyll layers of this type, which occur in association with the base of the euphotic zone, are common features of the California Current system (cf. Anderson, 1969 and Cullen, 1982). They may result from a number of processes such as an increase in phytoplankton biomass due to growth at the intersection of the euphotic zone and nutricline (Herbland and Voituriez, 1979). Two other possibilities are photoadaptation, where the chlorophyll per cell increases in response to low light conditions (Prezelin, 1981 and Beers et al 1975), or variability in fluorescence yield of the phytoplankton (Kiefer, 1982). At station E-4 and nearby stations the increase in beam c indicates increased biomass while the fluorescence per unit chlorphyll, or fluorescence yield, is relatively constant throughout the water column. However, the chlorophyll per unit beam c increases with depth at E-4 and suggests that the chlorophyll content per cell or per unit biomass also increases with depth.

To objectively examine CTZ data sets for the occurrence of phytoplankton layers which may have been moved out of the euphotic zone by subduction processes, it is necessary to differentiate the deep layers like those of Fig. 1 from those which probably result from in situ photosynthesis as in Fig. 2. Furthermore, it is necessary to rule out other processes which might also result in the presence of layers of fluorescent particles below the euphotic zone. A step in this process is to establish the relationship between the light field in the water column throughout the region and the vertical position of layers of phytoplankton.

The penetration of light into the water column is examined by comparing vertical profiles of PAR throughout the CTZ. A total of 17 stations from legs 1 and 2 of the Thomas Washington survey, all recorded within one hour of local noon, is used to examine the variability of the light field (Fig. 3A). Stations close to local noon were chosen in order to observe the maximum penetration of light into the water column. Following Huyer et al (1990), three regions are identified based on dynamic height (5/500 db): the jet corresponds to the range 0.82 to 0.96 m, inshore and southern waters below 0.82 m, and offshore and northern waters greater than 0.96 m. These ranges

are somewhat different from those used by Huyer et al (1990), but are more appropriate to the Thomas Washington data. Considerable variation in the depth of light penetration is found within the jet waters: typical values of the 1% light level in the most turbid waters are in the range of 20 to 30 db and are almost 80 db in the more clear waters (Fig. 3B). This depth range also spans that observed for the inshore and southern waters. Offshore waters are generally more clear with a typical 1% light level of about 85 db; much of the phytoplankton in the water column lies below this level.

Observations obtained during leg 2 of the Thomas Washington survey show that almost one third of the water column with high chlorophyll fluorescence levels ($\geq$ 1.0 volts) is found at depths below the 1% light level of the clearest offshore waters (Fig. 3C). About 6.4% occur below the 0.1% light level which ranges from about 115 to 125 db based on the three offshore profiles of Fig. 3B. The threshold fluorescence value of 1.0 v is chosen because it represents a high signal level; the noise level of the fluorometer and CTD acquisition system used on the Thomas Washington is about a factor of 4 smaller. The tail of the distribution of Fig. 3C extends down to 200 db, although layers exhibiting high fluorescence are found at depths exceeding 200 db in some of the other surveys. For stations within the jet, the fluorescence threshold used in producing the histogram of Fig. 3C corresponds to a chlorophyll concentration of about 1 μg/l and in the offshore waters to a level of about 0.3 μg/l. The points sorted into the histogram also have beam c values exceeding 0.4 m^{-1}. Thus much of the phytoplankton lies below the euphotic zone.

4. SUBDUCTION CRITERIA

Because phytoplankton require light for growth and reproduction, it is unlikely that local production of particles by photosynthesis can account for particle layers below the euphotic zone. These correspond to the hatched regions of Fig. 3B, particularly those below the 0.1% light level. This suggests that other processes are responsible for these deep layers such as vertical circulation out of the euphotic zone, particle sinking, resuspension of bottom sediments containing chlorophyll, or diapycnal mixing. We have no microstructure measurements to assess diapycnal mixing rates and assume that this is not an important mechanism for vertical particle transport here.

The hypothesis that vertical circulation, or subduction, accounts for these layers has been investigated by Kadko et al (1990) and is supported by a variety of indicators. In addition to high levels of chlorophyll, these layers often contain deficiences of ^{222}Rn ($\lambda_{1/2}$ = 3.85 days) with respect to ^{226}Ra activity, which indicates recent gas exchange with the atmosphere. The radon observations are perhaps the most unambiguous of all subduction indicators, since no other process can produce the deficiencies. The layers are often associated with local maxima in dissolved oxygen and often appear in water masses which are warmer and saltier than waters

above and below in θ-S diagrams. All of these observations are consistent with vertical movement of water masses away from the surface. However, a limitation of these indicators is that they are based on bottle sampling and therefore have very limited vertical resolution. Furthermore, the indicator ^{222}Rn is available for a relatively small number of stations and only as part of the Thomas Washington survey. In this analysis, we focus on the distributions of chlorophyll fluorescence and beam c as subduction indicators because they can be measured to about the same vertical resolution as CTD variables and because they are available from all surveys.

The possible role of particle sinking in forming the deep fluorescent layers is difficult to assess, although a number of factors suggest that it is not the dominant process. First, oceanic phytoplankton generally tend to sink slowly at vertical velocities of less than 1 m/day (Bienfang, 1981; Bienfang and Szyper, 1982; Bienfang et al 1982; Smayda, 1970). Observations from the Pt. Conception area of California indicate that phytoplankton sinking rates within 50 km of the upwelling center are ≤ 2 m/day (Bienfang, 1984). The estimates are much smaller than a suduction rate of 27 m/day obtained by Kadko et al (1990) based on ^{222}Rn samples. Second, θ-S relationships observed in these deep layers found in offshore regions of the jet appear related to those found nearshore in the euphotic zone, as is shown later. If particle sinking were dominant, then the θ-S relationship of a layer would have no correspondence to properties in the euphotic zone from which the particles were derived. The θ-S of the layer would simply be the local relationship at the time and depth at which the particle layer is observed as it sinks downward. Third, many of the deep regions of phytoplankton are in thin, well defined layers which are more or less Gaussian in shape (eg. Fig. 6F). A distribution of descending particles all falling at different rates (but strongly weighted toward large numbers of small particles (cf. Spinrad, 1986), for many days would tend to be spread vertically throughout the water column and would not concentrate in layers. Finally, in cross axis sections of the jet, where the station spacing is about 10 km, distributions of fluorescence and beam c approximately parallel σ_θ surfaces. This would not be expected if particle sinking across density surfaces were dominant.

It is possible that particle sinking may work in combination with subduction processes in layer formation. In nearshore areas where chlorophyll concentrations are large, particle coagualation effects may be important (Jackson, 1990) and could result in much higher sinking rates, greater than 100 m/day (Smetacek, 1985). However, the coagulated particles would have to have combined effective densities equal to the seawater density at some point in the water column to remain suspended. Otherwise they would sink to the bottom.

Another possible mechanism which might result in fluorescent particles appearing below the euphotic zone is resuspension of bottom sediments containing phytoplankton. Deep nepheloid layers due to resupension have been observed over the continental shelf off Oregon by Pak and Zaneveld (1977). Turbidity layers with high values of beam c are commonly observed below 100 m in all of the CTZ hydrographic

data sets, particularly nearshore. Typically these layers occur near the seafloor and exhibit no measurable fluorescence (eg. Figures 14D and 14E). However, deep turbidity layers from a few profiles exhibit very low, but measureable fluorescence signals. Comparison of signal levels indicates that the ratio of fluoresence to beam c is much lower in these bottom resuspended layers than in the phytoplankton layers higher in the water column. These layers are easily differentiated because their θ-S relationships are very different from those found anywhere in the euphotic zone and the corresponding seawater densities are much greater.

Based on the preceeding analysis, we conclude that the phytoplankton layers observed well below the euphotic zone, which exhibit high values and correlated distributions of fluorescence and beam c, result primarily from subduction processes. However, some clarification about "well below the euphotic zone" is required. The presence of phytoplankton below the 1% light level at a specific station does not necessarily mean that the phytoplankton were not produced in situ, because the depth of light penetration can change. For example, a layer of phytoplankton might initially grow near the deepest observed 1% light level of 80 to 90 db in clear water. After this growth, energetic near-surface advection could transport a second, more shallow layer of particles, over the deeper layer and produce a much shallower 1% light level. The result would be a deep layer of phytoplankton produced in situ which is observed below the euphotic zone. Other scenarios might also produce a similar situation. For this reason we generally limit our analysis to those layers found below the deepest 0.1% light levels which are found in clear, offshore waters. We have used a pressure of 120 db, about the midpoint of the range in 0.1% light levels in offshore waters (Fig. 3C), to represent this point in the water column. While this is a very restrictive criteria it does reduce the possibility that the observed particles result from in situ photosynthesis.

To objectively search each of the CTZ data sets for subducted water masses we applied three criteria based on the preceding analysis. If all three of the following criteria are satisfied, we consider it very likely that the water mass has been subducted. The criteria are: 1) pressure $\geq$ 120 db, 2) beam c $\geq$ 0.4 m^{-1}, and 3) fluorescence signal exceeds the instrumental noise level. For these data, a beam c threshold of 0.4 m^{-1} or larger is found to differentiate turbid layers from more clear ambient waters. Minimum observed levels of beam c in individual profiles from all of the data sets fall in the range 0.35 - 0.40 m^{-1} and are taken to be representative of the effective clear water values of beam c (c_w). This range of c_w falls within that given by Lavelle and Baker (1987) of 0.31 - 0.42 m^{-1}. The range is also comparable to two experimental results for c_w presented by Jerlov (1976, Table XIII): 0.319 and 0.385 m^{-1} (interpolated to 660nm).

The threshold fluorescence signal level had to be determined individually for each of the surveys because the effective noise level for each fluorometer and CTD data acquisition system was different. The procedure for determining this threshold is subjective and is

based on comparing signal levels in fluorescent layers with minimum observed levels which are taken to be the instrumental noise level. Minimum signal thresholds are derived from all of the survey data and are used in identifying subducted water massses. It proved impractical to use a uniform chlorphyll or total pigment concentration as a criteria for these data because of high scatter in the observed relationship between fluorescence voltage and pigment concentrations derived from bottle samples. Much of this scatter is apparently due to regional differences in the regression coefficients and may result from differences in phytoplankton species composition (Hood, 1990).

To search for subducted water masses, all of the CTZ data sets were sorted based on the criteria developed above. Profiles from all surveys identified as containing subducted layers were individually examined to verify that noise spikes or other data problems were not present. This sorting procedure also identified a few layers near the sea floor with relatively high beam c, but very weak fluorescence levels that barely exceeded the threshold. Water properties of these points are typical of the ambient deep water and they are usually found at depths exceeding 300 m. These points were excluded from the analysis.

5. DISTRIBUTION OF SUBDUCTED WATER MASSES

Subducted water masses occur frequently in the CTZ based on the numbers of profiles from each grid survey which contain them (Fig. 4). They are found both in the seaward flowing jet and nearshore, and a few are found in offshore waters south of the jet. Beam c and fluorescence anomalies in the layers from these latter profiles were very weak as were all of the layers in the first survey. In the first three surveys from 20 June - 18 July, no layers are found in offshore waters to the north and east of the jet and those farthest offshore during this time are in the jet itself. A different situation is observed during the fourth survey from 21-27 July when subducted layers are found near the offshore boundary of the grid. They are also seaward of the strongest flow in the jet. Over the time period from the third to fourth grid surveys, the orientation of the jet rotated abruptly from offshore flow to along shore flow where it remained constant at least through the end of the fifth survey. The change in orientation coincided with a general relaxation in the wind field at this time (Stanton et al, 1990), a pattern which has been observed previously in the same area (Strub et al, 1990).

Leg 2 of the Thomas Washington survey was designed to sample selectively the seaward flowing jet and is therefore useful for examining the distribution of subducted water masses here. In addition, this survey included some stations outside of the jet for comparison. Application of the criteria developed in Section 4 shows that subducted water masses are found frequently out along the jet axis with the most seaward of these stations lying almost 300 km from Pt. Arena (Fig. 5). A few stations south of Pt. Arena and inshore of the jet are located in an anti-cyclonic eddy (Swenson and Niller, 1990) and also contain subducted water masses.

Profiles from a group of five stations from those identified in Fig. 5 suggest a gradual sinking of phytoplankton layers along isopycnal surfaces out the jet axis (Fig. 6A). These stations were not occupied sequentially and do not follow any particular water parcel in a Lagrangian sense. Rather, they illustrate where particle layers can be found in different regions of the jet. At the near shore station 46, high levels of fluorescence and beam c are observed above 80 db. Radon deficiencies at this station indicate recent gas exchange throughout this depth range (Kadko et al, 1990) even though no surface mixed layer is present. Surface mixed layers in density are apparent only at offshore stations 67 and 33 in the upper 20 db. Out the axis of the jet, beam c, fluorescence, and chlorophyll levels are frequently high on and above the 25.8 isopycnal, which deepens from about 23 db at station 46 to 150 db at station 33. Discrete layers around this level are evident (Figures 6C, 6E, and 6F), but are not continuous in profiles from nearby stations. Measureable beam c and fluorescence levels are not limited to the depth of the 25.8 isopycnal and above, but exceed 200 dbar in some stations such as 17A (Fig. 6D) and in stations from the five grid surveys as well.

Figure 6 suggests that the vertical distribution of phytoplankton layers may be related to the position of isopycnal surfaces. Because of this we use an isopycnal coordinate system in much of the following analysis. In particular, the distributions of properties on two isopycnal surfaces are examined in some detail: (1) the 25.8, which frequently lies within the euphotic zone; and (2) the 26.2, which is generally below the euphotic zone.

Comparison of the distributions of beam c and pressure on isopycnal surfaces indicates that the lateral extent of subducted regions may be large. Offshore, where the 25.8 surface is below 120 db, beam c $\geq$ 0.4 m^{-1} at stations 33, 34, 72, and 75 (Figures 7A and 7B); the along axis separation of the 33-34 pair and the 72-75 pair is about 50 km while the cross axis dimension of this layer of particles is at least 28 km. The pattern of isopycnal contours of fluorescence (not shown) is very similar to that for beam c in Fig. 7A. The highest levels of beam c (c $\geq$ 0.7 m^{-1}) on the 25.8 isopycnal occur inshore where this surface lies within the euphotic zone (above 50 db based on Fig. 3B) and is consistent with in situ production of phytoplankton. One of these areas where the 25.8 isopycnal is warped upwards is centered on 124.25 W, 38.75 N and results from the combination of the southward jet flow and the strong northward flow due to the anticyclonic eddy (Fig. 14 E).

A very different situation occurs on the deeper 26.2 isopycnal where the highest levels of beam c (c $\geq$ 0.5 m^{-1}) are found nearshore at depths below 120 db (Figures 8A and 8B), except for the area immediately south of Pt. Arena which is very shallow. Farther offshore and west of 125.5 W, all points having c $\geq$ 0.4 m^{-1} lie below 120 db. Again the pattern of fluorescence on this surface (not shown) is very similar. We conclude from this that most of the phytoplankton found on the 26.2 isopycnal in the area covered by the survey were not produced in situ where observed, but instead, have

been moved vertically and horizontally by subduction and advection processes out of the euphotic zone in their source regions. This suggests that subduction processes play an important role in govering water mass properties on this isopycnal surface. In contrast, in situ production within the survey area may account for much of the phytoplankton on the 25.8 surface near shore.

6. SOURCES OF SUBDUCTED WATER MASSES

The distribution of beam c and fluorescence on iopycnals like the 26.2 indicate that many of the deep phytoplankton layers probably originate in the euphotic zone away from where they are observed. Because isopycnals slope steeply upward toward the coast in the CTZ area, some lie within the euphotic zone near shore, but at much greater depths farther offshore (Figures 7B and 8B). We hypothesize that these inshore areas where the isopycnals rise into the euphotic zone are the major source regions for the phytoplankton and subducted water masses, although some sources probably lie to the north of the area covered by the surveys. Use of the term "source region" for subducted water masses simply means that they were near the surface there.

If the deep phytoplankton layers originate near shore, then the θ-S relationships in the layers found offshore should be similar to those near shore in the euphotic zone if isopycnal and diapycnal mixing rates are not too large and if particle sinking is not important. For purposes of tracing vertical water mass movement, the phytoplankton act as a dye which identifies water masses which have previously been in the euphotic zone. The θ-S characteristics are potentially useful for tracing horizontal movement of these water masses if remote source regions can be unambiguously identified in θ and S. In contrast to θ and S which are conservative away from the mixed layer, beam c and fluorescence levels are likely to change substantially since phytoplankton concentrations are non-conservative over time scales of a few days and levels change due to a variety of processes such as photosynthesis and grazing by zooplankton. Therefore, the usefulness of fluorescence and beam c as vertical water mass tracers will be limited by their effective decay rates.

In the remainder of this section, the θ-S characteristics of subducted water masses are compared with those of potential source regions for two (overlapping) time periods: first, over the entire experimental period including the time when the jet orientation changed rapidly (late July to early August); and second, during the time when the jet orientation was fairly stable (late June to mid-July). Higher resolution sampling from the Thomas Washington during this latter period allows more detailed inferences to be drawn regarding nearshore source regions.

The locus all θ-S points from the five grid surveys of Fig. 4 which satisfy the subduction criteria of Section 4 cluster into two areas of distinct characteristics (Fig. 9A). Most of the points fall

within a σ_θ range 25.9 - 26.6 (Group A) while a second group is clustered between 25.1 - 25.5 (Group B). Most of the points in the second group are found at the offshore stations in Fig. 4D when the jet orientation changed abruptly. The exception is offshore station 163 (Fig. 4B) from the first Pt. Sur survey which also falls in Group B. The differences in θ-S characteristics of Group B suggest that the subducted layers found offshore, particularly after the jet reorientation, are not derived from the same sources as those found elsewhere.

Subducted water masses corresponding to the main group of points (Group A) in Fig. 9A are probably derived from nearshore sources based on comparisons with upper ocean θ-S characteristics in the CTZ area. All θ-S points in the upper 50 db of the water column from each inshore line of the grid surveys are plotted in Fig. 9B along with the envelope of points from the subducted layers shown in Fig. 9A. The extensive overlap of the Group A θ-S points with points from the inshore lines is consistent with nearshore source regions for the subducted water masses. In contrast, very little overlap is found between the (Group A) subducted layer θ-S points and those from all of the other (offshore) lines from the grid surveys (Fig. 9C). The upper 50 db of the water column is chosen because this range falls within the euphotic zone throughout most of the survey area (Fig. 3). Howver, this may underestimate the depth range of the euphotic zone in nearshore areas since some of the θ-S points in the subducted layers correspond to higher densities than found nearshore above 50 db.

It is also likely the majority of the subducted water masses observed within the jet during the process sampling from the Thomas Washington (Fig. 5) result from nearshore sources. During this sampling, the position and water mass composition of the jet were fairly constant for about a month covering the period 20 June to 18 July (Huyer et al, 1990). The consistent orientation of the jet may be seen in the first three geopotential anomaly fields of Fig. 4. Most of the θ-S points within the subducted layers of the jet, identified in Fig. 5, fall within the Group A envelope of θ-S points in Fig. 9A. However, a few such as those from Station 35 which is located far offshore, fall within the Group B envelope and may indicate another source farther offshore (Figures 10A and 10B).

The θ-S points for the subducted water masses within the jet are consistent with formation by isopycnal mixing of waters from different nearshore source regions. Based on θ-S distributions in the upper 50 db of the water column, two potential source regions are the waters offshore and north of Pt. Arena (and possibly north of the study area), represented by station A3, and waters immediately north of Pt. Reyes, represented by station A13 (Fig. 10B). Points lying between the A3 and A13 curves could be formed by advection and isopycnal mixing between these two source regions. However, source water contributions from the area around Pt. Reyes require a northward coastal flow inshore of the jet. The θ-S curves of Fig. 10B are obtained from leg 1 data of the Thomas Washington survey (25 June - 2 July) and show that waters on the southern end of the inshore line are

saltier on a given isopycnal than those to the north. This situation persisted during all of the grid surveys based on isopycnal plots of "spiciness" presented by Huyer et al (1990).

A detailed θ-S diagram (Fig. 10C) containing only points in subducted water masses below 120 db which lie on σ_θ = 26.2 shows that θ-S points at stations 9A and 47, in the strong southward flow of the jet (Fig. 10A), are very similar to those at Station A3 located north of Pt. Arena. In contrast, at stations 51 and 52, which are in strong northward flow (Fig. 14C), θ-S points are nearly identical to those at Station A13 located just off Pt. Reyes. The remaining points lie between these end members.

Further evidence that Pt. Reyes may be a source region for some of the subducted layers is the distribution of S on σ_θ = 26.2 from legs 1 and 2 of the Thomas Washington survey. Salinities exceeding 33.82 are found on two lines of stations that extend offshore from just south of Pt. Arena (Fig. 11); these points generally are found below 90 db (Fig. 8B) and have high levels of beam c (Fig. 8A) and fluorescence. Two of these stations, 51 and 52, satisfy the subduction criteria of Section 4. The high salinity of these waters (S ≥ 33.82) is consistent with northward (and downward) advection from the Pt. Reyes area along the 26.2 isopycnal. The more comprehensive inshore survey (leg 1) shows that S ≥ 33.82 on σ_θ = 26.2 at three stations (A11, A12, and A13) near Pt. Reyes, but nowhere to the north (Fig. 12A). In this same area, this isopycnal reaches vertically to within about 40 db of the surface at station A13 (Fig. 12B) and has c ≥ 0.8 m^{-1} (Fig. 12C). Thus, waters found near Pt. Arena below 120 db, such as stations 51 and 52, may originate in the upper ocean off Pt. Reyes where similar S, beam c, and fluorescence (not shown) characteristics are found.

7. VERTICAL TRANSPORT BY ISOPYCNAL SINKING AND MIXING

One mechanism that could result in vertical movement of water masses out of the euphotic zone and subsequent transport offshore to depths exceeding 120 db is simply flow along sloping isopycnal surfaces out the axis of the jet. Evidence for water mass sinking in the jet comes from a sequence of CTD stations made daily alongside a surface drifter (path shown with solid line in Fig. 13A). Averages of density in the upper 10 m of the water column progressively decrease and the total change from the beginning to the end of the track is about 0.7 kg/m^3. Fluid particles traveling on the 25.8 or 26.2 isopynal surfaces could experience depth changes of well over 100 m based on the distributions of pressure of these surfaces (Figures 7B and 8B). A particle moving on a density surface would probably not change depth monotonically because local depth variations result from processes like mesoscale eddy activity.

The time required for a water particle to move out the jet axis on a particular isopycnal varies greatly because of strong vertical shear in the jet. Depending upon the mean advective speed and the depth of a particular isopycnal, the time scale for this process to occur

ranges from a several days to a few weeks. This advective time scale is of interest because it puts a lower bound on the persistence time for the subduction indicators used in this analysis (beam c and fluorescence) and it gives an estimate of the order of magnitude of typical vertical velocities. To illustrate how this isopycnal sinking out of the euphotic zone might proceed, the advection times and vertical and horizontal velocities are computed along hypothetical drifter tracks located on the 25.8 and 26.2 isopycnal surfaces.

Advective time scales for flow along these isopycnals are estimated from 8 sections of geostrophic velocity which cross the jet at approximately right angles to the flow (Fig. 13A). The sections were obtained over a two week period (7 - 21 July) during the time when the position of the jet was relatively constant (Huyer et al 1990). Geostrophic velocity profiles are computed from adjacent pairs of stations on these transects and use a reference level of 500 db. Some sections show sloping σ_θ surfaces down to 500 db so actual velocities may be larger. Geostrophic velocities are then interpolated onto the isopycnals based on the average pressure of the given isopycnal for each pair of stations; examples of isopycnal velocity profiles on σ_θ = 26.2 are shown in Figures 13B to 13E. Negative velocities indicate generally southward or offshore flow and the shapes of the profiles are approximated by polynomial fits to data points from station pairs.

On the two inshore lines 47 - 53 and 65 - 57, regions of strong lateral shear separate the southward flowing jet from the region of northward flow of the anti-cyclonic eddy (Fig. 13B and 13C). The region of southward flow in the eddy is barely resolved on the east end of each line. Farther out the jet along the line of stations 17A -21, the flow field has smaller lateral shear and is offshore everywhere in the profile (Fig. 13D). The mean velocity from this profile is -0.14 m/s. The offshore flow of the jet is still detectable at the most offshore line 73 - 76, 360 km from shore, and shows smaller lateral shear with a mean velocity of -0.11 m/s.

Advective time and velocity scales along the hypothetical drifter tracks at three levels in the jet are summarized in Table 1. Mean velocity and time scales are based on averages of only the portions of each profile which are in the jet; eddy or recirculating portions of isopycnal velocity profiles are not included in the means. The minimum time scales and maximum velocity scales are based on the maximum jet velocity in each section. The end points for the hypothetical drifter tracks are stations 48 and 75 and the track length is 321 km (dotted line, Fig. 13A). The hypothetical drifter on the 25.8 isopycnal begins at about 20 db at station 48, well within the euphotic zone, and requires from 12 to 21 days to reach station 75 where it would be at about 140 db. The corresponding times on the 26.2 surface are about double these times while those at 5 db are about half. For comparison, the track of an actual surface drifter is also shown in Figure 13A (solid line). This drifter took 5.1 days to travel from station 6 to station 32 which compares favorably with minimum and mean times (between stations 48 and 32A) of 4.5 - 9.8 days using the geostrophic velocities at 5 db/500 db in the cross-jet

sections of Fig. 13A.

Another physical process which can transport water masses vertically out of the euphotic zone is mixing along sloping isopycnal surfaces. This is distinguished from isopycnal advection because it produces changes in water properties. Isopycnals and isohalines tilt in association with the geostrophic velocity field (Figures 7B and 8B) and can have slopes as large as 0.005 in the high vorticity region between the jet and anti-cyclonic eddy (Figures 14A, 14B, and 14C); cross-axis displacement in this lateral shear zone would produce large vertical excursions.

Isopycnal mixing is suggested by the scatter of θ-S points in subducted water masses in Figures 10B and 10C and is clearly evident in the θ-S profile at station 50 (Fig. 15) located on the edge of the high vorticity region in Fig. 14C. Waters at station 50, from the northward flowing part of the anti-cyclonic eddy, are warmer and saltier than southward flowing jet water of the same density at station 47. This difference in properties is in agreement with the comparison between jet and inshore water masses of Huyer et al (1990). The cusp in the θ-S curve between 15 and 50 db at station 50 extends over to the curve at station 47 and is consistent with isopycnal advection and mixing between the jet and the eddy. Not only are the θ-S characteristics different in this 35 db thick layer, but beam c and fluorescence are also lower and more characteristic of those in the jet at station 47 just below σ_θ = 26.2 (Figures 14D and 14E). This region of high relative vorticity between the jet and the eddy (Fig. 13B and 14C) is where isopycnal mixing processes might be expected to be strong.

Additional pieces of evidence for isopycnal mixing between the eddy and jet are nearly linear relationships between S and c (and fluorescence) on certain isopycnals like the 26.2 (Fig. 16A). Changes in beam c are proportional to particle concentrations, among other factors, (cf. Spinrad 1986, Baker and Lavelle, 1984, and Bishop, 1986) and scalar-like behavior is expected if non-conservative effects like grazing and particle sinking are not too strong. The linear relationship is consistent with end member mixing between water masses with c-S properties similar to those at stations 49 and 50; that is high salinity water in the eddy (hatched region, Fig. 14B) mixing with lower salinity jet water (stippled region, Fig. 14B). Beam c differences are similar on the 26.2 surface (Fig. 14C) with $c \leq 0.5^{-1}$ at stations 48, 49 and 50 and $c \geq 0.5^{-1}$ at stations 51 and 52. While a (nearly) linear θ-S relationship must obtain on isopycnals, this need not be true for c and S because particle concentrations are too low to affect seawater density.

Points in Fig. 16 which depart significantly from the linear trend are those in the eddy center (station 52) and in the southward flowing part of the eddy (station 53), both outside the high vorticity region. The pressure change resulting from isopycnal mixing may be as large as 50 db here (Fig. 14A) and is sufficient to transport particles out of the euphotic zone. The maximum euphotic zone depth across the section of Fig. 14 is about 60 db and occurs at station 52 where PAR is

measured within 1 hour of local noon. This is the maximum depth because overlying beam c and fluorescence levels, and hence particle concentrations, are the lowest for the section (Figures 14C and D). Note that isopleths of beam c and fluorescence approximately follow the changing depths of σ_θ contours (eg. 26.2).

To acquire more degress of freedom and test for a significant linear trend between c and S in the high vorticity region (stations 47-51), c-S points on the 26.2 surface were combined with those from the 26.15 and 26.25 surfaces (lower stippled region, Fig. 14A). A scatter plot of ΔS versus Δc (Fig. 16B) shows a significant linear correlation where, $\Delta S = (S-\bar{S})/\sigma_s$. Here $\bar{S}$ is the mean and σ_s is the standard deviation for salinity on each of the three surfaces; the same procedure is used in computing Δc. In this band of isopycnal surfaces c-S points in the southward jet flow are all fresher and less turbid than those in the northward eddy flow (solid symbols, Fig. 16B). This is not true for a more shallow set of three isopycnals, 25.75, 25.80, and 25.85 (upper stippled region, Fig. 14A) where mixed c-S properties are flowing in both directions. The linear c-S trend is also less significant on these surfaces and may result from more than two water mass types mixing together or increased particle production since these isopycnals are within the euphotic zone.

8. *DISCUSSION AND CONCLUSIONS*

Shipboard CTD and bio-optical observations made during the summer upwelling season in 1988 reveal the presence of deep phytoplankton layers below the euphotic zone in many areas of the coastal transition zone (CTZ), including a strong baroclinic jet which was present throughout the observational period. A principal conclusion of this study is that the water masses associated with the phytoplankton have been moved downward by subduction processes. This finding is supported by the distributions of several hydrographic and geochemical tracers, including ^{222}Rn, chlorophyll, and dissolved oxygen (Kadko, et al 1990). Criteria to objectively identify subducted water masses have been developed and are based on the light field in the water column and levels of fluorescence and the beam attenuation coefficient (beam c). Subducted water masses are observed in all five hydrographic grid surveys of the CTZ experiment which covered the period 20 June - 4 August, 1988.

The θ-S relationships corresponding to the subducted water masses fall into two distinct groups and are consistent with two near surface subduction regions, one nearshore and a second much farther offshore. The scatter in θ-S points suggests that the nearshore source is distributed in space and has contributions from the area in the vicinity of Pt. Reyes and from an area north of Pt. Arena, or possibly north of the study area. Subducted water masses from the nearshore source region were present throughout the experimental period, while those from the offshore source were most frequently observed just after the strong baroclinic jet changed orientation from offshore to alongshore flow.

A variety of physical processes may lead to water mass subduction and we hypothesize that one mechanism is movement along sloping isopycnal surfaces due to advection or mixing processes. Drifter observations of Brink et al (1990) show that convergence zones exist offshore in the jet which result in downwelling velocities of order 10 m/day. This process could account for the subducted water masses that are due to offshore sources.

The positions of layers of phytoplankton in the water column indicate that some layers sink along isopycnal surfaces as they are advected out the jet axis. Vertical sinking rates based on geostrophic flow on sloping density surfaces are 6-10 m/day for the 25.8 surface and 2-4 m/day for the deeper 26.2 surface. These estimates are based on advection over 320 km of the jet axis and probably underestimate maximum vertical velocities. This is because isopycnals rise up into higher velocity flow nearshore where isopycnal slopes are generally the largest. Kadko et al (1990) estimate vertical velocities as high as 27 m/day based on ^{222}R deficiences. Advective time timescales out the jet axis are about 2-3 weeks along the 25.8 surface and about double this along the 26.2 surface. This suggests that detectable levels of beam c and fluorescence from subducted phytoplankton can persist for several weeks. Evidence for isopycnal mixing processes is based on θ-S relationships and observed linear correlations between beam c and salinity on density surfaces in a region of high vorticity on the jet boundary. In this coastal upwelling system, particles (phytoplankton) can apparently be mixed like other scalars such as salinity, a result found by Washburn et al (1989) in the vicinity of the North Pacific Subtropical Front.

ACKNOWLEDGEMENTS

Ken Brink provided helpful comments on an early draft of the manuscript. This work was supported by the Office of Naval Research, Coastal Sciences Program.

REFERENCES

Anderson, G.G., 1969, Subsurface chlorophyll maximum in the Northeast Pacific Ocean, Limnol. Oceanogr., 14, 386-391.

Baker, E.T., and J.W. Lavelle, 1984, The effect of particle size on the light attenuation coefficient of natural suspension, J. Geophys. Res., 89, C5, 8197-8203.

Beers, J.R., F.M.H. Reid, and G.L. Stewart, 1975, Microplankton of the NOrth Pacific central gyre. Population structure and abundance, June 1973, Int. Rev. Gesamten Hyrobiol., 60, 607-638.

Bienfang, P., J. Szyper, and E. Laws, 1982, Sinking rate and pigment responses to light-limitation of a marine diatom: implications to

dynamics of chlorophyll maximum layers, Oceanol. Acta, 6, 1, 55-62.

Bienfang, P., and J. Szyper, 1982, Effects of temperature and salinity on sinking rates of the centric diatom Ditylum Brightwelli, Bio. Oceangr., 1, 3, 211-223.

Bienfang, P.K., 1981, Sinking rate dynamics of Cricosphaera Carterae Braarud. 1. Effects of growth rate, limiting substrate, and diurnal variations in steady-state populations, J. Exp. Mar. Ecol., 49, 217-233.

Bishop, J.K.B., 1986, The correction and suspended particulate matter calibration of Sea Tech transmissometer data, Deep-Sea Res., 33, 1, 121-134.

Brink, K.H., R.C. Beardsley, P.P. Niiler, M. Abbott, A. Huyer, S. Ramp, T. Stanton, and D. Stuart, 1991, Statistical properties of near surface flow in the California coastal transition zone, J. Geophys. Res., (this issue).

Cullen, J.J., 1982, The deep chlorophyll maximum: comparing vertical profiles of chlorophyll a, Canadian J. of Fisheries and Aquatic Sci., 39, 791-803.

Davis, R.E., 1985. Drifter observations of coastal surface currents during CODE: the statistical and dynamical views, J. Geophys. Res., 90, 4756-4772.

Flament, P.J., A. Armi, and L. Washburn, 1985, The evolving structure of an upwelling filament, J. Geophys. Res., 90, 11,765-11,778.

Hood, R., 1990, Phytoplankton biomass, photosynthetic light response, and physical structure in a Northern California upwelling system, Ph.D. dissertation, Scripps Institution of Oceanography.

Huyer, A., F. Chavez, T. Cowles, J. Fleischbein, P.M. Kosro, S. Ramp, L. Small, T. Stanton, and L. Washburn, 1990, Evolution of the Coastal Transition Zone off Northern California, June to August 1988, submitted to J. Geophys. Res.

Jackson, G., 1990, A model of formation of marine algol flocs by physical coagulation processes, in press, Deep-Sea Res.

Jerlov, H.G., 1976, Marine Optics, Elsevier, New York, 231 pp.

Kadko, D.C., L. Washburn, and B.H. Jones, 1990, Evidence of subduction within cold filaments of the N. California coastal transition zone, submitted, J. Geophys. Res.

Kiefer, D.A., 1973, Fluorescence properties of natural phytoplankton populations, Mar. Bio., 22, 263-269.

Pak, H., J.R.V. Zaneveld, 1977, Bottom nepheloid layers and bottom mixed layers observed on the continental shelf off Oregon during the

upwelling season, J. Geophys. Res., 82, 3921-3931.

Prezelin, B.B., 1981, Light reactions in photosynthesis, Physiological bases of phytoplankton ecology, Canadian Bulletin of Fisheries and Aquatic Sci. (T. Platt, Ed.), 210, 1-43.

Smayda, T.J., 1970, The suspension and sinking of phytoplankton in the sea, Oceanogr. Mar. Biol. Ann. Rev., 8, 353-414.

Smetacek, V.S., 1985, Role of sinking in diatom life-history cycles: ecological, evolutionary, and geological significance, Mar. Bio., 84, 239-251.

Spinrad, R.W., 1986, A calibration diagram of specific beam attenuation, J. Geophys. Res., 91, C6, 7761-7764.

Stanton, T.P., J. Stockel, M.L. Batteen and S. Ramp, 1990, Upper ocean response to a wind relaxation event in the coastal transition zone, submitted to J. Geophys. Res.

Strub, P.T. and the CTZ Group, 1991, The nature of the cold filaments in the California Current System, submitted to J. Geophys. Res.

Swenson, M., P.P. Niiler and K. Brink, 1990, The dynamical and thermodynamical structure of the flow associated with a cold filament off Pt. Arena, California in July 1988, submitted to J. Geophys. Res.

Table 1. Advection along Jet Axis*

Level	Time (days) Minimum - Mean	Horizontal Velocity (m/s) Maximum - Mean	Vertical Velocity (m/day) Maximum - Mean
p = 5db	5 - 11	0.70 - 0.33	
σ_θ =			
25.8	12 - 21	0.30 - 0.17	10 - 6
26.2	20 - 42	0.18 - 0.09	4 - 2

*stations: 48-62-88-19-26-39-32A-75
Total distance = 321 km

FIGURE CAPTIONS

Fig. 1A. Locations of stations E4 and 6. Contours of geopotential anomaly (0/500 db) are from first Pt. Sur survey, 6 - 12 July 1988.

Fig. 1B. Profiles of photosynthetically available radiation (PAR), beam c, and fluorescence at station 6 along with chlorophyll concentrations at discrete depths.

Fig. 1C. Profiles of potential temperature, potential density, and salinity at station 6.

Fig. 2A. As in 1B, but for station E4.

Fig. 2B. As in 1C, but for station E4.

Fig. 3A. Location of PAR profiles obtained within one hour of local noon (triangles). Contours of geopotential anomaly (0/500 db) are from first Pt. Sur survey, 6 - 12 July 1988. Offshore extension of geopotential anomaly contours from Thomas Washington survey.

Fig. 3B. PAR profiles obtained within one hour of local noon in: the offshore jet (solid lines), southern and inshore waters (dotted lines), and offshore waters (dashed lines). Vertical bar shows range in 1% light level in jet. Arrows indicate depths of 1% and 0.1% light levels in offshore waters.

Fig. 3C. Histogram showing distribution of fluorescence in water column from all CTD profiles obtained during leg 2 of Thomas Washington survey.

Fig. 4. Locations of stations containing subducted water masses during: (A) first Wecoma survey, 20-27 July; (B) first Pt. Sur survey, 6-12 July; (C) second Pt. Sur survey, 12-18 July; (D) third Pt. Sur survey, 21-27 July; (E) and second Wecoma survey, 29 July - 4 August. Contours of geopotential anomaly (0/500 db).

Fig. 5. Locations of all stations during leg 2 of Thomas Washington survey (triangles). Filled triangles indicate stations with subducted water masses. Contours of geopotential anomaly (0/500 db) are from first Pt. Sur survey, 6 - 12 July 1988. Offshore extension of geopotential anomaly contours from Thomas Washington survey.

Fig. 6A. Locations of profiles in jet shown in Figures 6B to 6F.

Fig. 6B. - 6F. Profiles of potential density, beam c, and fluorescence along with chlorophyll concentrations at five stations along jet axis.

Fig. 7A. Horizontal contour section of beam c on σ_θ = 25.8.

Fig. 7B. Horizontal contour section of pressure on σ_θ = 25.8.

Fig. 8A. Horizontal contour section of beam c on σ_θ = 26.2.

Fig. 8B. Horizontal contour section of pressure on σ_θ = 26.2.

Fig. 9A. θ-S points corresponding to subducted water masses from all five grid surveys (Fig. 4). Water masses of points in Group A are from nearshore sources and Group B from offshore sources.

Fig. 9B. θ-S points in upper 50 db of water column for the most inshore lines of all five grid surveys. Envelope of θ-S points of subducted water masses in Group A (Fig. 9A) shown by dashed lines.

Fig. 9C. θ-S points in upper 50 db of water column for all offshore lines of all five grid surveys. Envelope of θ-S points of subducted water masses (Fig. 9A) shown by dashed lines.

Fig. 10A. Locations of various stations whose θ-S relationships are shown in Figures 10B and 10C.

Fig. 10B. θ-S profiles for inshore stations on line A (solid lines) and θ-S points for subducted water masses observed below 120 db (open circles) during leg 2 of Thomas Washington survey.

Fig. 10C. θ-S points of subducted water masses on σ_θ = 26.2 and θ-S profiles for upper 50 db at stations A3 and A13 (solid lines).

Fig. 11. Horizontal contour section of salinity on σ_θ = 26.2 from leg 2 of Thomas Washington surey.

Fig. 12. Horizontal contour sections on σ_θ = 26.2 from leg 1 of Thomas Washington survey of: A. salinity, B. pressure, C. beam c.

Fig. 13 A. Cross-jet transects used for computing sections of geostrophic velocity. Track of surface drifter indicated with solid line and hypothetical drifter track with dotted line.

Fig. 13B. - 13E. Isopycnal profiles of geostrophic velocity on σ_θ = 26.2 for: (B) stations 47 - 53, (C) stations 65 - 57, (D) stations 17A - 21, and (E) stations 76 - 73.

Fig. 14A. Vertical section for stations 47 - 55 of $@1s$%$@1q (see Fig. 13A for station locations). 1% light level at station 52 indicated with arrow.

Fig. 14B. As in 14A, but for salinity. Dashed line shows 26.2 isopycnal. Stippled area indicates parts of $@1s$%$@1q = 26.2 for S $\leq$ 33.8 and hatched area parts for S $\geq$ 33.8.

Fig. 14 C. Vertical section of geostrophic velocity computed from stations 47 - 53. Stippled areas indicate flow to the south.

Fig. 14D. As in 14A, but for beam c.

Fig. 14E. As in 14A, but for fluorescence.

Fig. 15. θ-S profiles for stations 47 and 50.

Fig. 16A. Salinity - beam c diagram for stations 47 - 53 on σ_θ = 26.2. Filled circles indicate stations in southward jet flow and open circles indicate stations in northward anti-cyclonic eddy flow. Station 52 is near the center and 53 in the southward flow of the eddy (triangles).

Fig. 16B. Salinity - beam c diagram (non-dimensionalized) for points on: A. σ_θ = 26.15 (squares), B. 26.20 (circles), and C. 26.25 (triangles). Filled symbols indicate points in northward jet flow. Solid line is a least squares fit.

Fig. 16C. As in 16B, but on: A. σ_θ = 25.75 (squares), B. 25.80 (circles), and C. 25.85 (triangles).

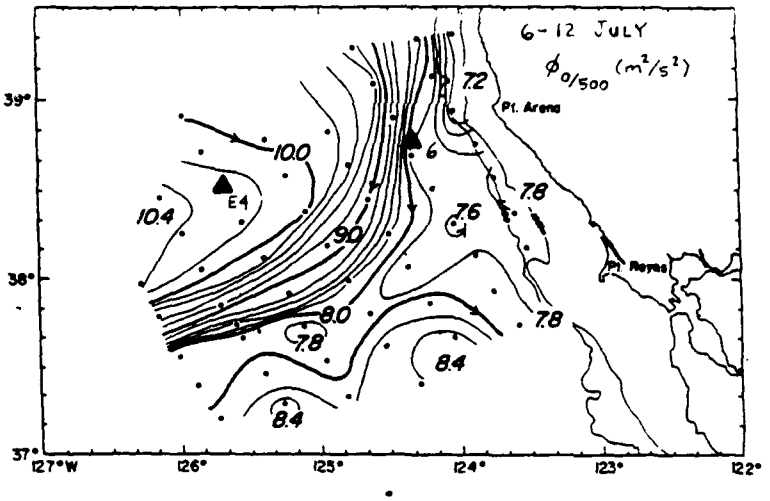
6-12 JULY
$\phi_{0/500}$ (m^2/s^2)
Pt. Arena
Pt. Reyes
E4
10.0
10.4
9.0
8.0
7.8
8.4
7.2
6
7.6
7.8
7.8
8.4
39°
38°
37°
127°W
126°
125°
124°
123°
122°

A.

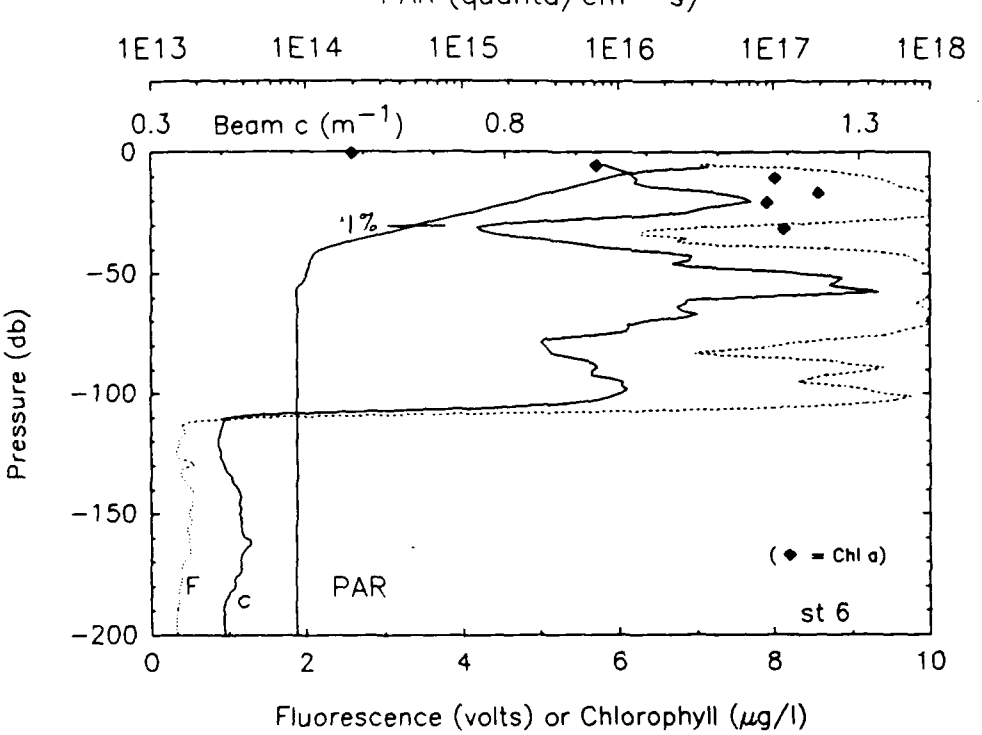
PAR (quanta/cm^2-s)
1E13
1E14
1E15
1E16
1E17
1E18
0.3
Beam c (m^{-1})
0.8
1.3
0
-50
-100
-150
-200
Pressure (db)
1%
F
c
PAR
(◆ = Chl a)
st 6
0
2
4
6
8
10
Fluorescence (volts) or Chlorophyll (μg/l)

B.

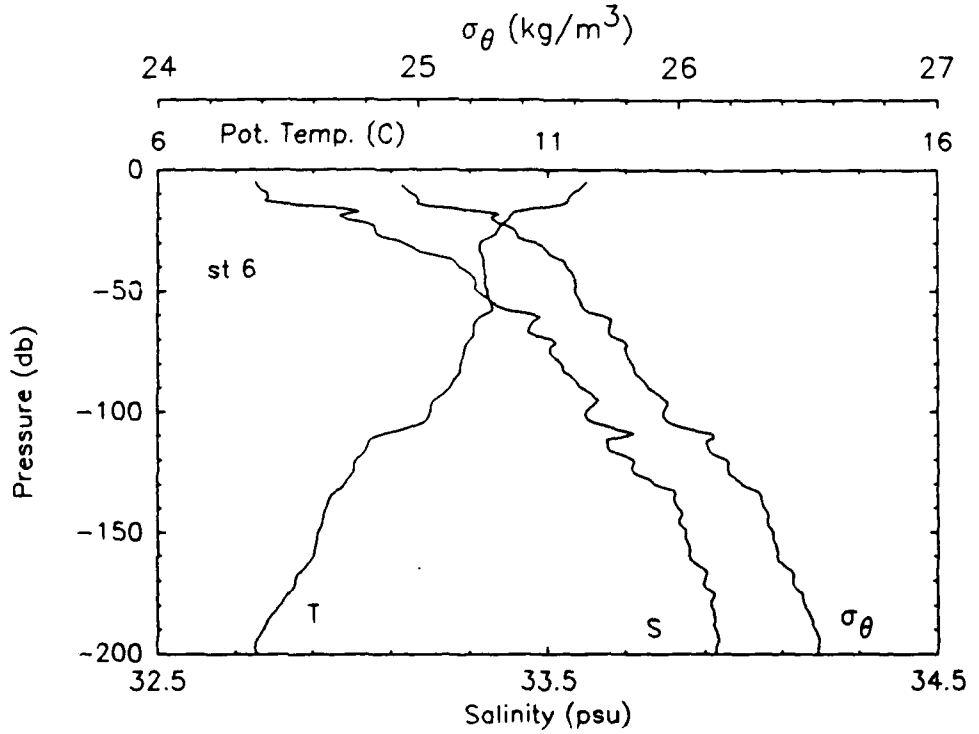
σ_θ (kg/m^3)
24
25
26
27
6
Pot. Temp. (C)
11
16
0
-50
-100
-150
-200
Pressure (db)
st 6
T
S
σ_θ
32.5
33.5
34.5
Salinity (psu)

C.

FIG. 1

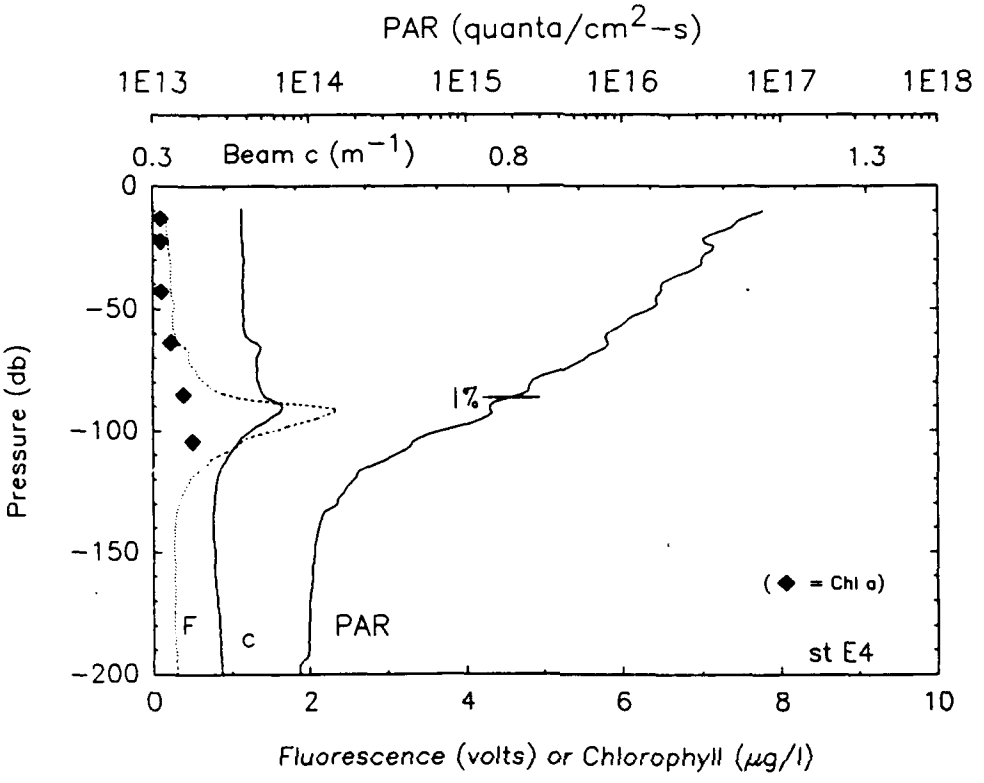
PAR (quanta/cm^2-s)
1E13
1E14
1E15
1E16
1E17
1E18
0.3
Beam c (m^{-1})
0.8
1.3
0
-50
-100
-150
-200
Pressure (db)
1%
(◆ = Chl a)
F
c
PAR
st E4
0
2
4
6
8
10
Fluorescence (volts) or Chlorophyll (μg/l)

A.

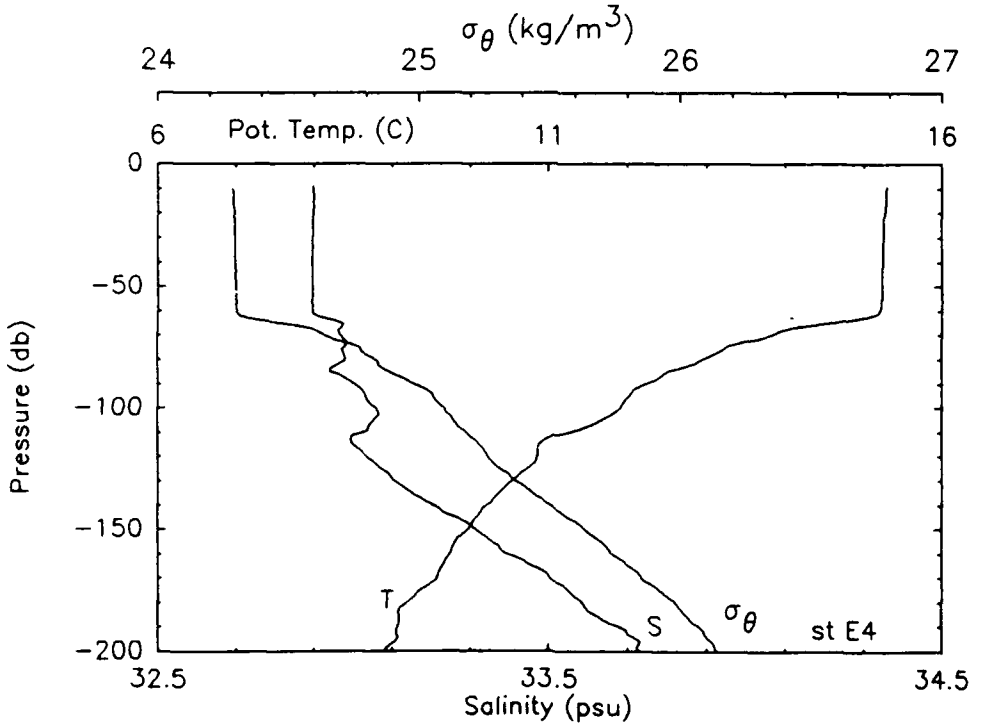
σ_θ (kg/m^3)
24
25
26
27
6
Pot. Temp. (C)
11
16
0
-50
-100
-150
-200
Pressure (db)
T
S
σ_θ
st E4
32.5
33.5
34.5
Salinity (psu)

B.

FIG. 2

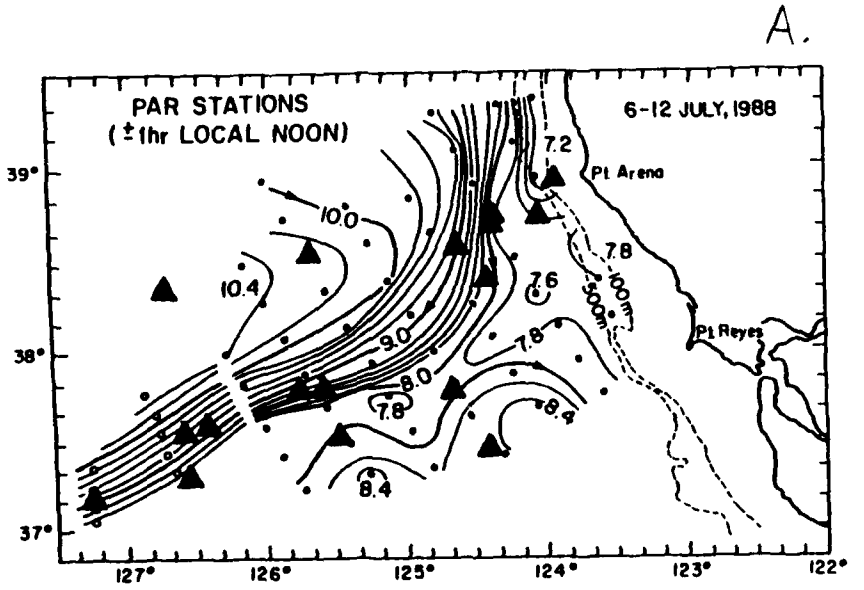
A.
PAR STATIONS
(±1hr LOCAL NOON)
6-12 JULY, 1988
Pt Arena
Pt Reyes
100m
500m
10.0
10.4
9.0
8.0
7.8
7.6
7.2
8.4
39°
38°
37°
127°
126°
125°
124°
123°
122°

FIG. 3

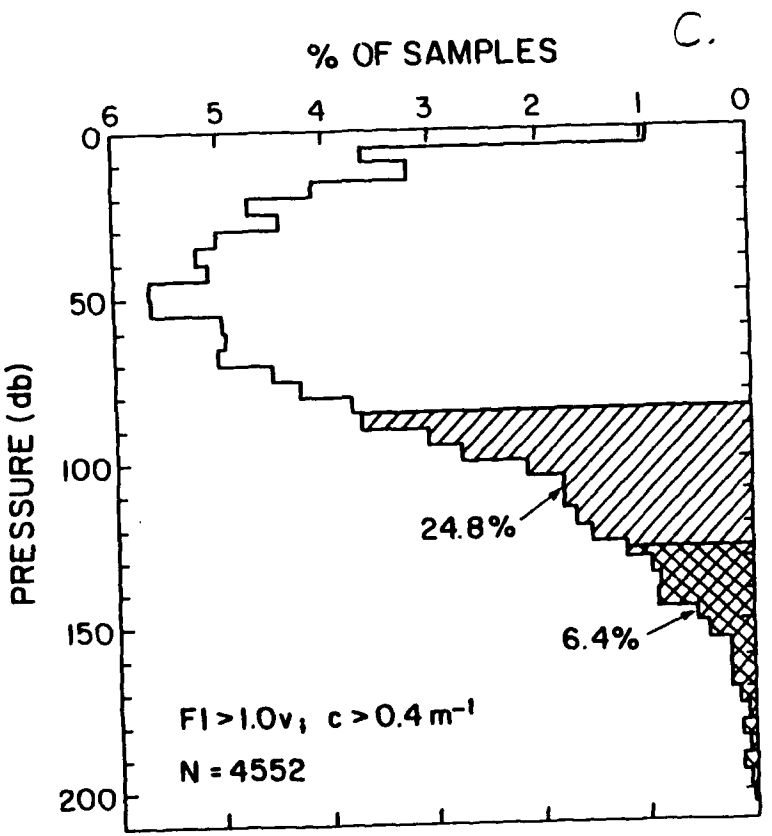
C.
% OF SAMPLES
6 5 4 3 2 1 0
PRESSURE (db)
0
50
100
150
200
24.8%
6.4%
Fl>1.0v; c>0.4 m⁻¹
N = 4552

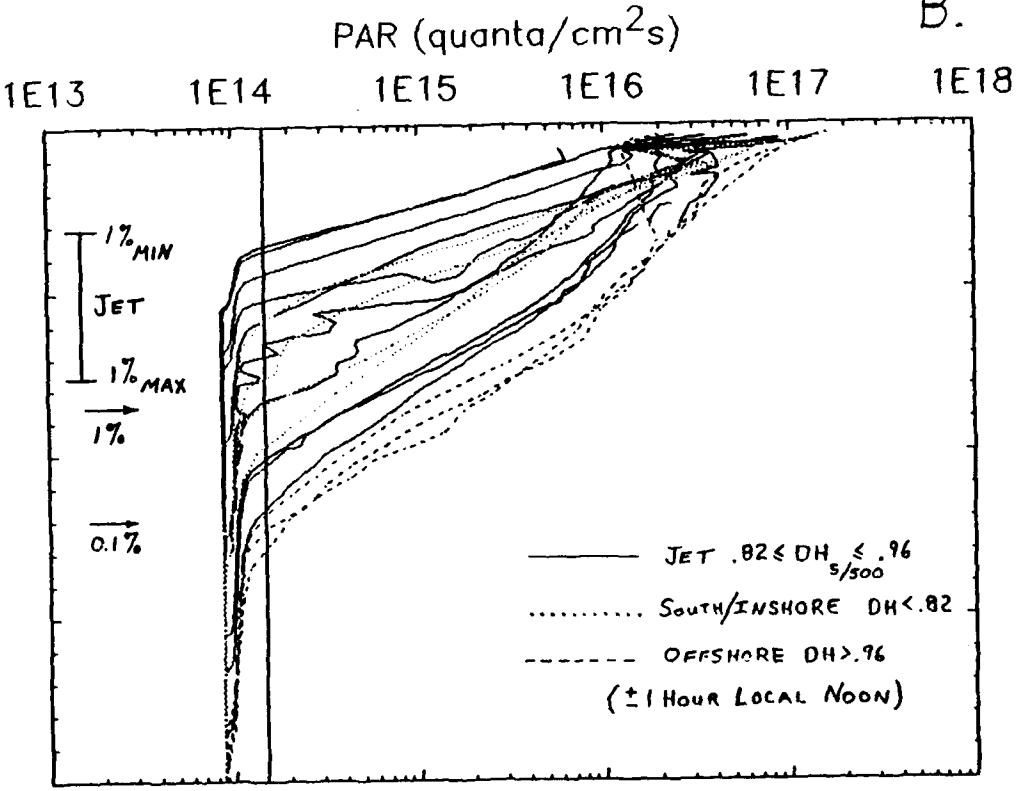
B.
PAR (quanta/cm²s)
1E13 1E14 1E15 1E16 1E17 1E18
1%MIN
JET
1%MAX
1%
0.1%
JET .82 ≤ DH s/500 ≤ .96
SOUTH/INSHORE DH<.82
OFFSHORE DH>.96
(±1 HOUR LOCAL NOON)

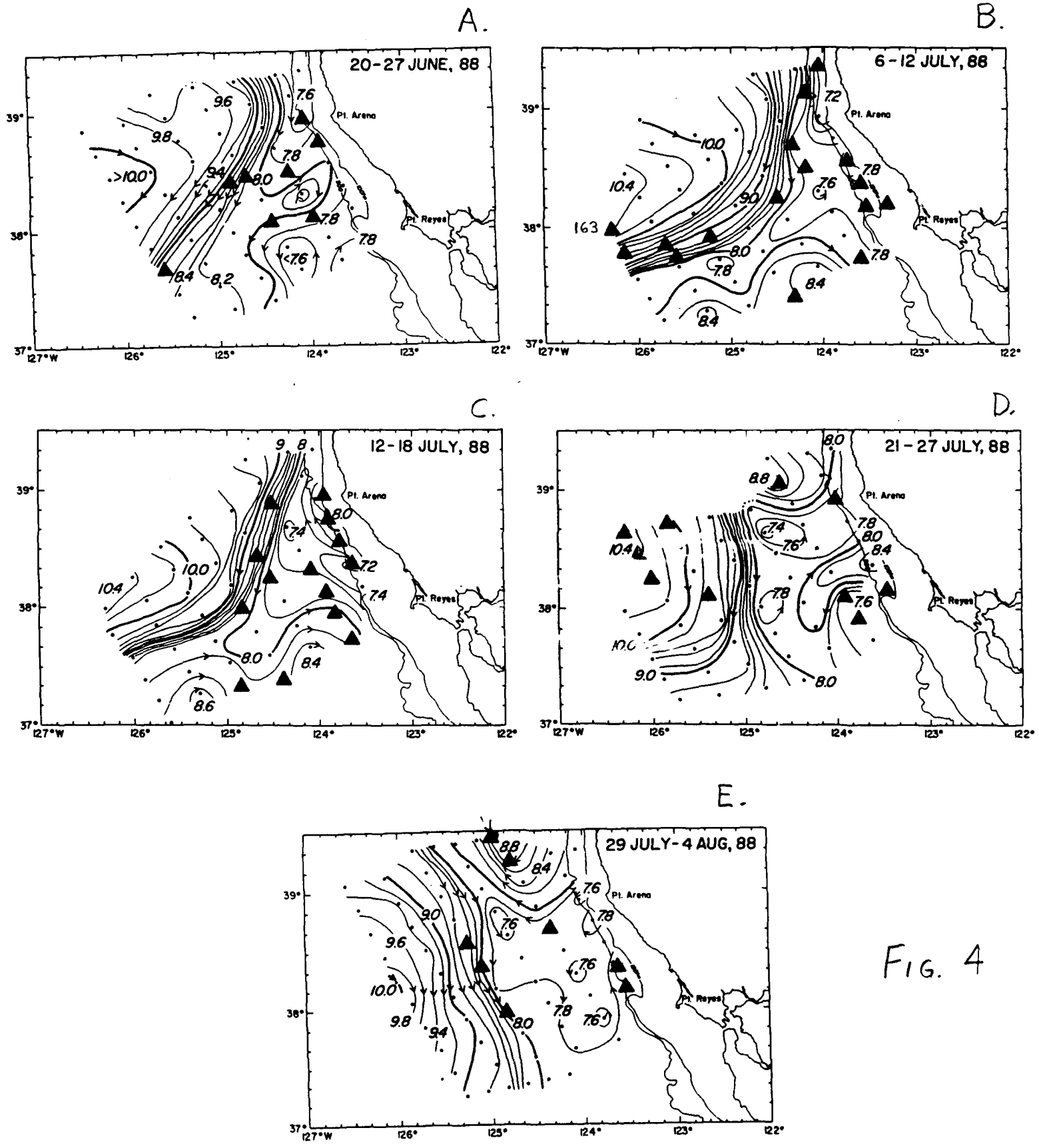
A.
20-27 JUNE, 88
B.
6-12 JULY, 88
C.
12-18 JULY, 88
D.
21-27 JULY, 88
E.
29 JULY-4 AUG, 88
Pt. Arena
Pt. Reyes
39°
38°
37°
127°W
126°
125°
124°
123°
122°

FIG. 4

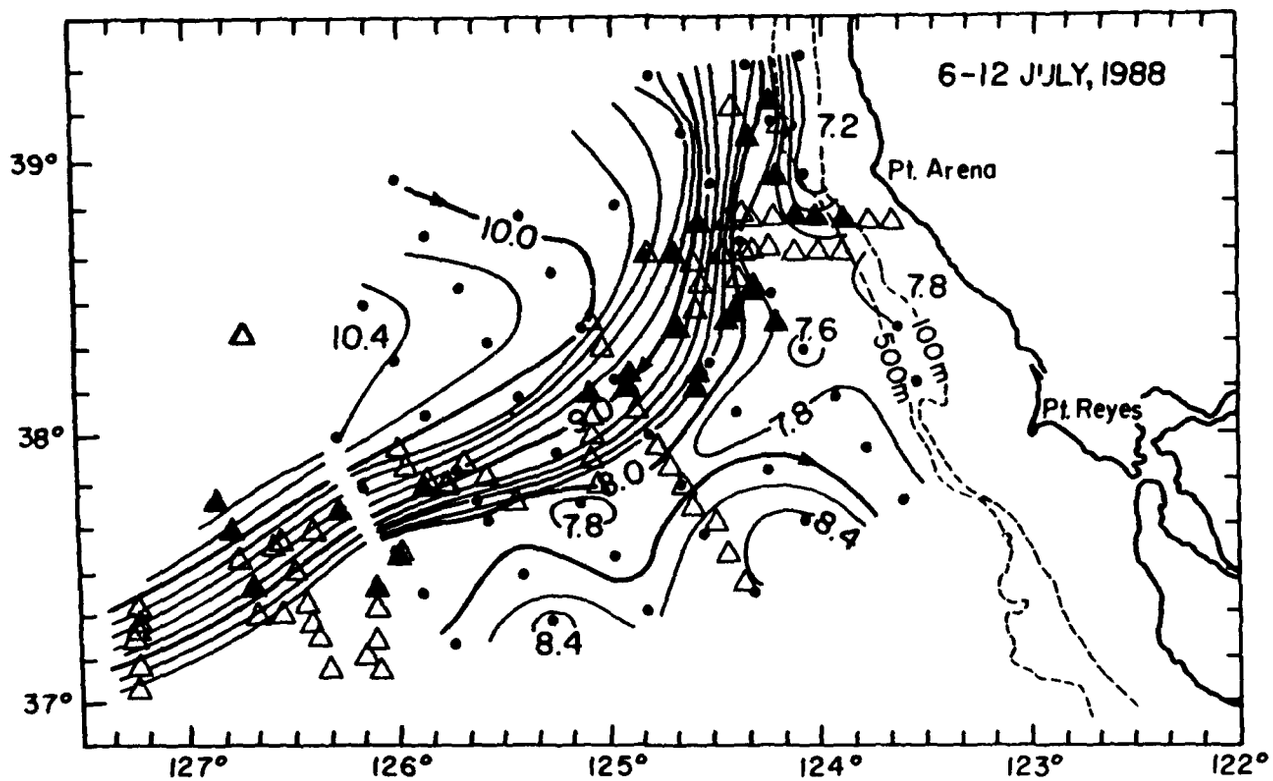
6-12 JULY, 1988
Pt. Arena
Pt. Reyes
100m
500m
39°
38°
37°
127°
126°
125°
124°
123°
122°
10.0
10.4
9.0
8.0
7.8
8.4
7.2
7.6
7.8
7.8
8.4

FIG. 5

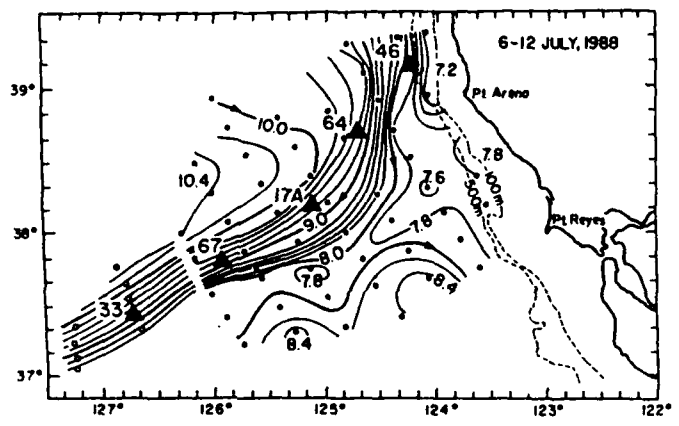
A.
6-12 JULY, 1988
Pt Arena
Pt Reyes
39°
38°
37°
127°
126°
125°
124°
123°
122°
46
7.2
64
10.0
10.4
17A
9.0
67
8.0
7.8
7.6
7.8
8.4
33
100m
500m

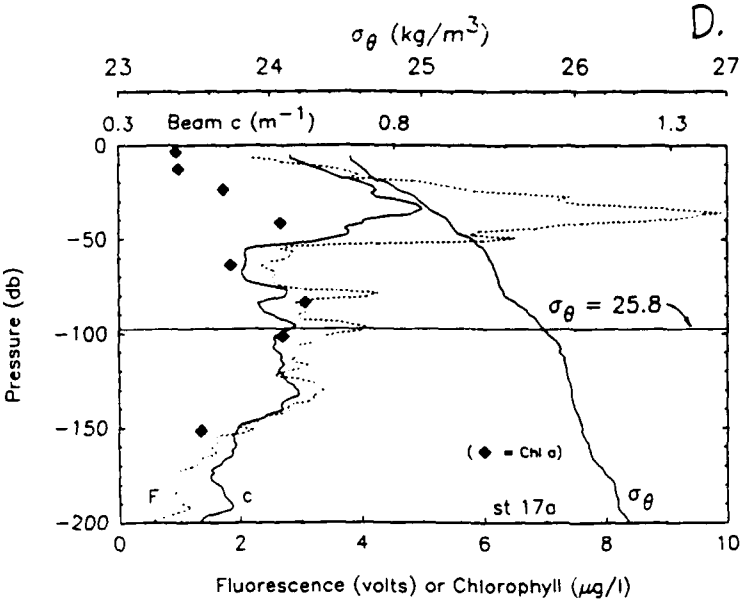
D.
σ_θ (kg/m^3)
23 24 25 26 27
0.3 Beam c (m^{-1}) 0.8 1.3
Pressure (db)
0 -50 -100 -150 -200
σ_θ = 25.8
(◆ = Chl a)
F
c
st 17a
σ_θ
0 2 4 6 8 10
Fluorescence (volts) or Chlorophyll (μg/l)

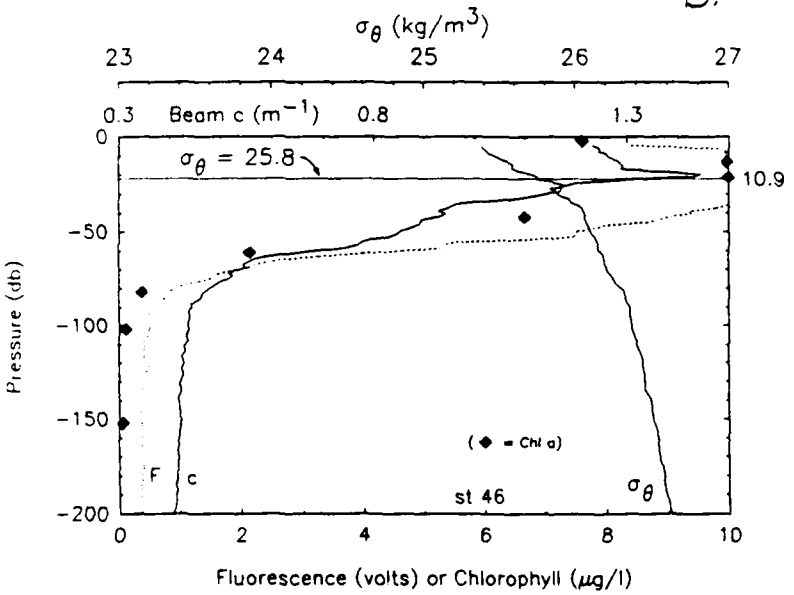
B.
σ_θ (kg/m^3)
23 24 25 26 27
0.3 Beam c (m^{-1}) 0.8 1.3
Pressure (db)
0 -50 -100 -150 -200
σ_θ = 25.8
10.9
(◆ = Chl a)
F
c
st 46
σ_θ
0 2 4 6 8 10
Fluorescence (volts) or Chlorophyll (μg/l)

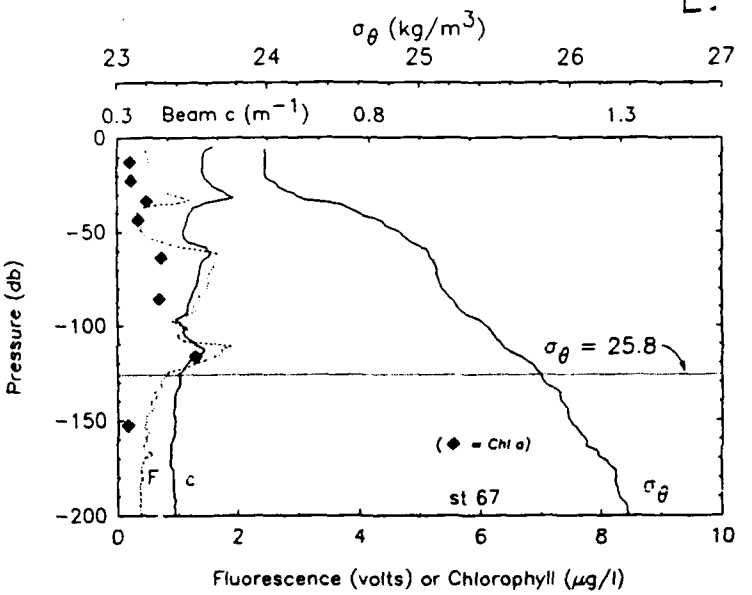
E.
σ_θ (kg/m^3)
23 24 25 26 27
0.3 Beam c (m^{-1}) 0.8 1.3
Pressure (db)
0 -50 -100 -150 -200
σ_θ = 25.8
(◆ = Chl a)
F
c
st 67
σ_θ
0 2 4 6 8 10
Fluorescence (volts) or Chlorophyll (μg/l)

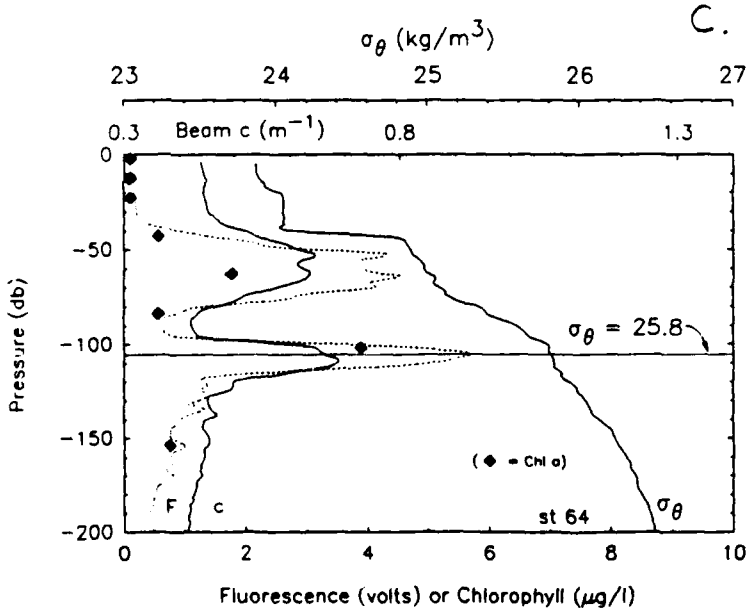
C.
σ_θ (kg/m^3)
23 24 25 26 27
0.3 Beam c (m^{-1}) 0.8 1.3
Pressure (db)
0 -50 -100 -150 -200
σ_θ = 25.8
(◆ = Chl a)
F
c
st 64
σ_θ
0 2 4 6 8 10
Fluorescence (volts) or Chlorophyll (μg/l)

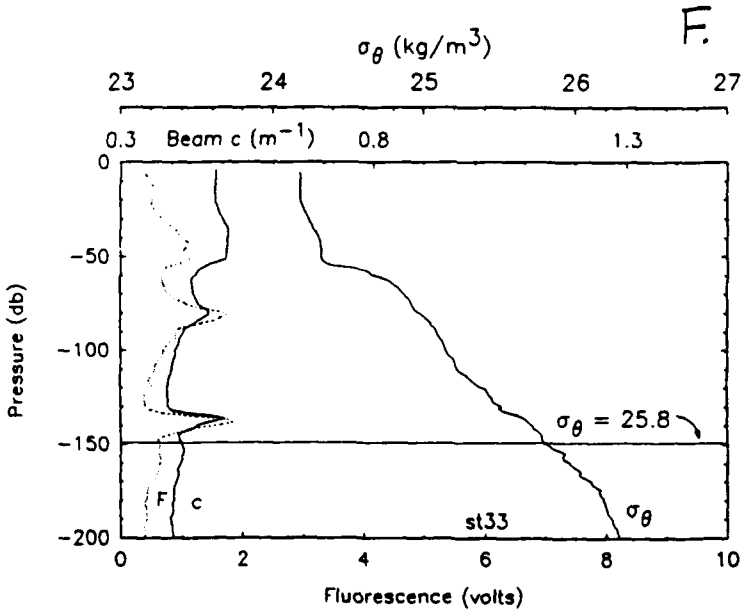
F.
σ_θ (kg/m^3)
23 24 25 26 27
0.3 Beam c (m^{-1}) 0.8 1.3
Pressure (db)
0 -50 -100 -150 -200
σ_θ = 25.8
F
c
st33
σ_θ
0 2 4 6 8 10
Fluorescence (volts)

FIG. 6

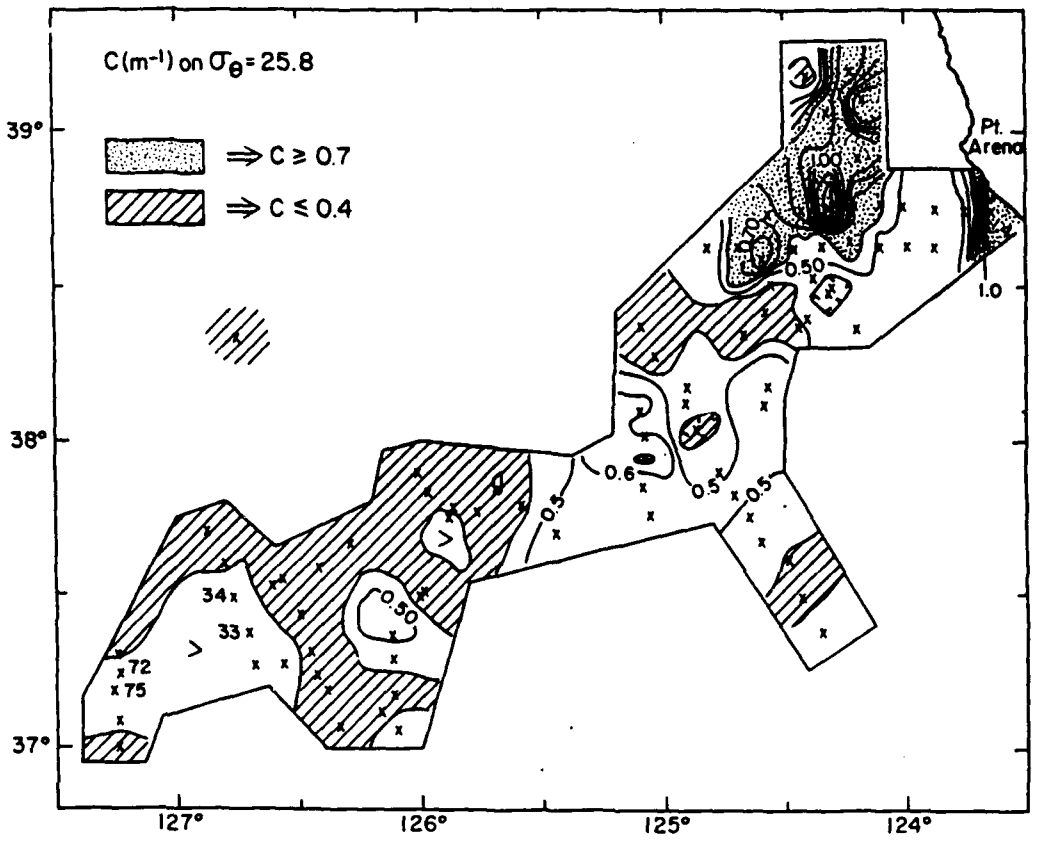
C(m⁻¹) on σθ = 25.8
⇒ C ≥ 0.7
⇒ C ≤ 0.4
Pt. Arena
39°
38°
37°
127°
126°
125°
124°
1.0
0.50
0.6
0.5
0.5
0.5
0.50
34
33
72
75

A.

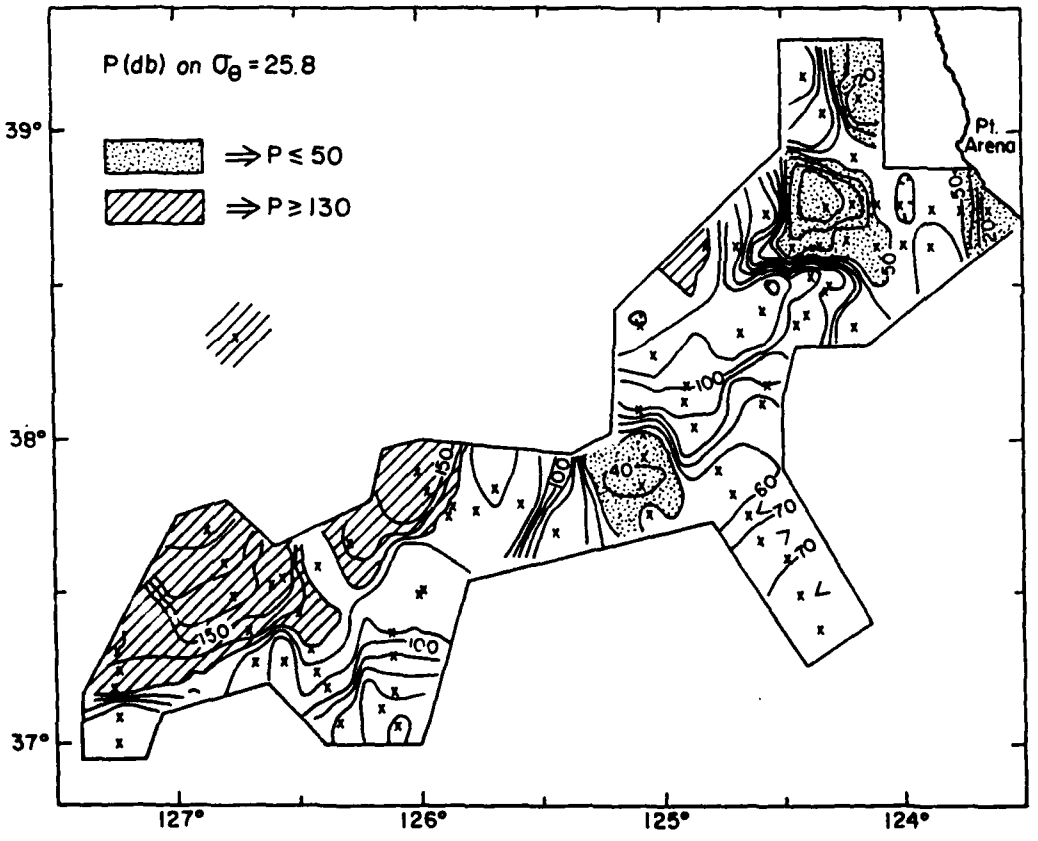
P (db) on σθ = 25.8
⇒ P ≤ 50
⇒ P ≥ 130
Pt. Arena
39°
38°
37°
127°
126°
125°
124°
100
40
60
70
150
100

B.

FIG. 7

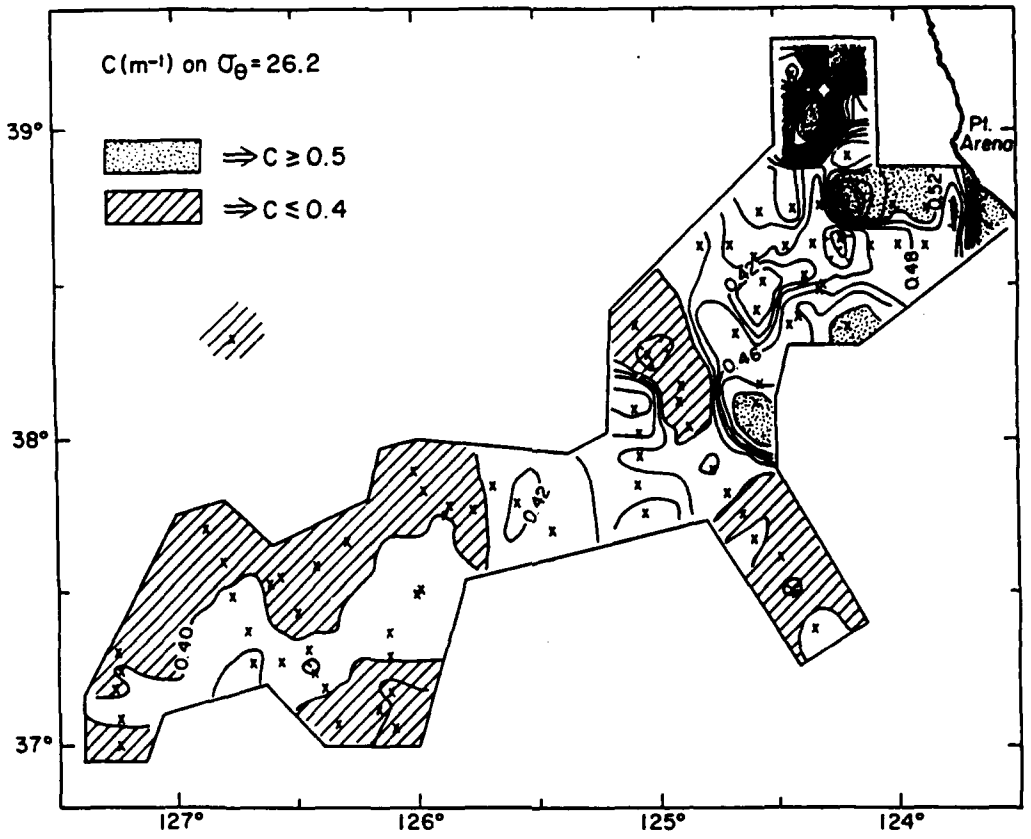
C(m⁻¹) on σθ = 26.2
⇒ C ≥ 0.5
⇒ C ≤ 0.4
Pt. Arena
39°
38°
37°
127°
126°
125°
124°
0.52
0.48
0.46
0.42
0.40

A.

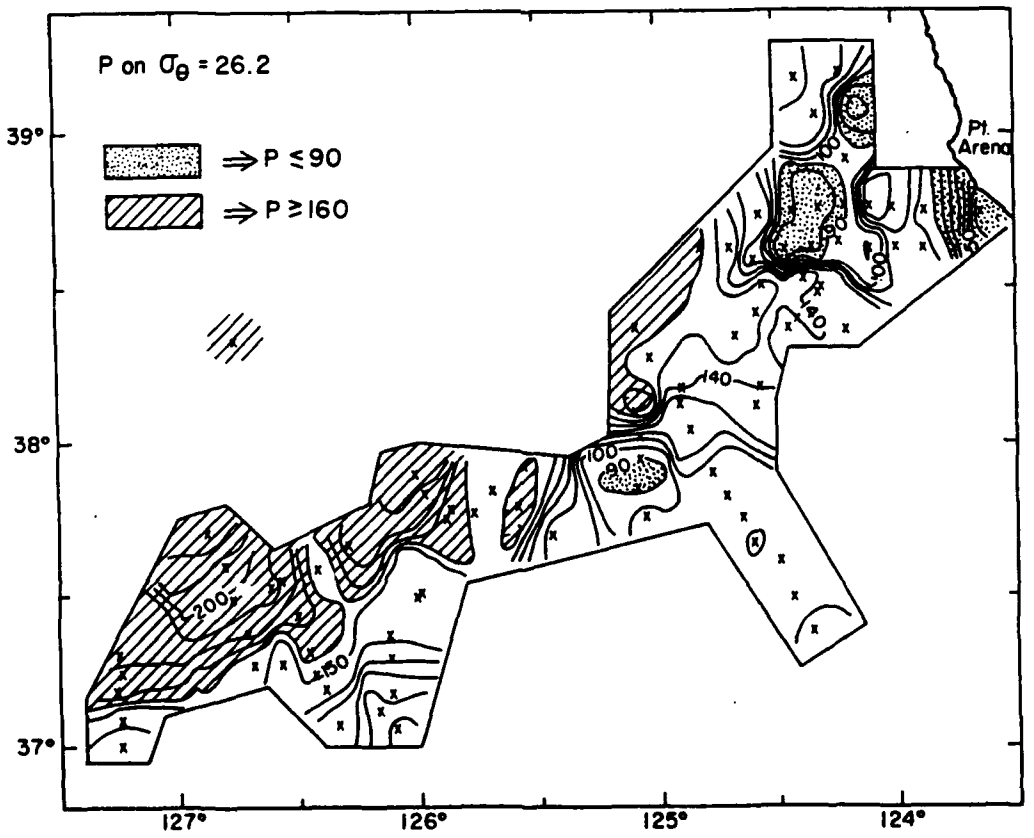
P on σθ = 26.2
⇒ P ≤ 90
⇒ P ≥ 160
Pt. Arena
39°
38°
37°
127°
126°
125°
124°
200
150
100
90
140

B.

FIG. 8

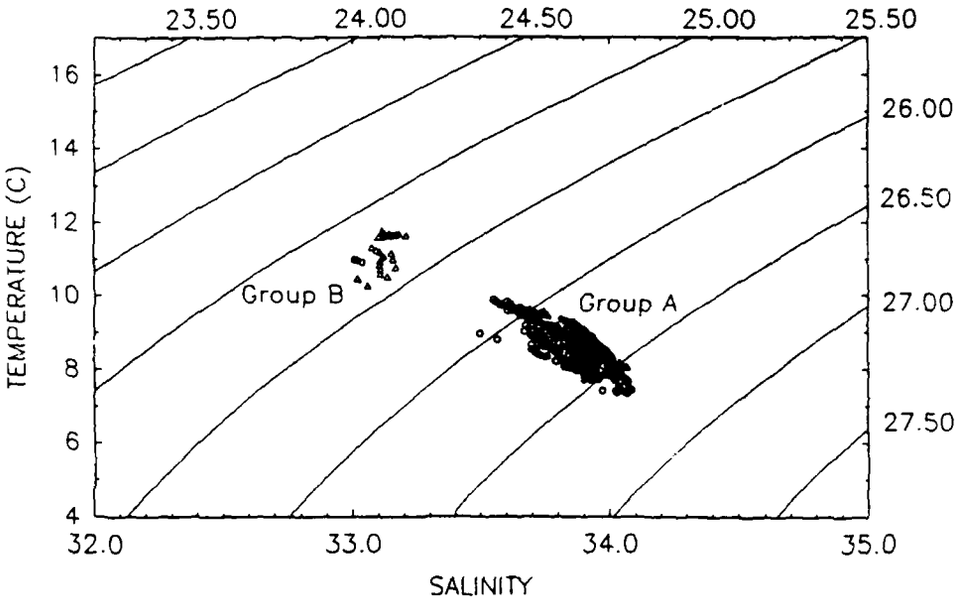
23.50
24.00
24.50
25.00
25.50
16
14
12
10
8
6
4
TEMPERATURE (C)
26.00
26.50
27.00
27.50
Group B
Group A
32.0
33.0
34.0
35.0
SALINITY

A.

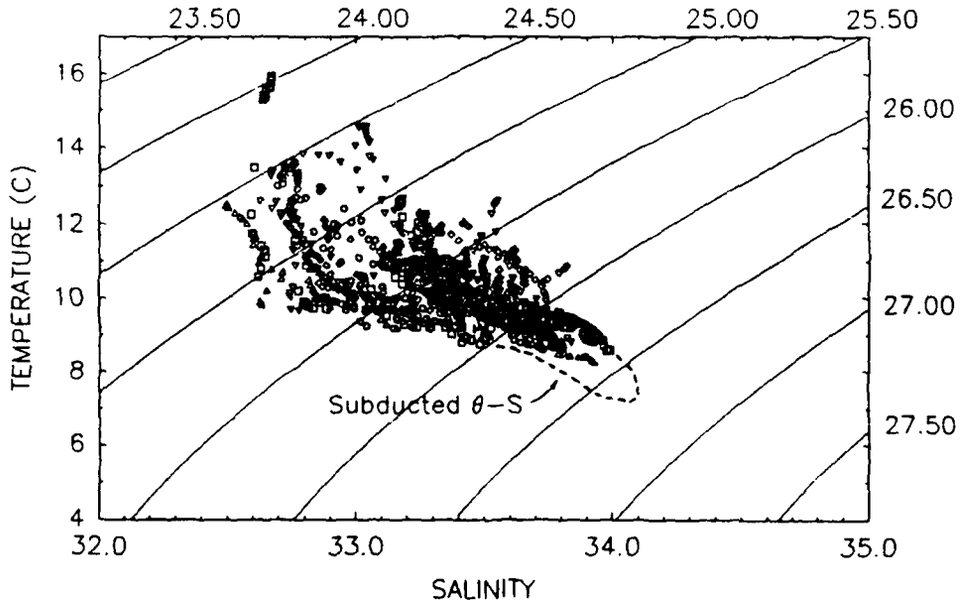
23.50
24.00
24.50
25.00
25.50
16
14
12
10
8
6
4
TEMPERATURE (C)
26.00
26.50
27.00
27.50
Subducted θ–S
32.0
33.0
34.0
35.0
SALINITY

B.

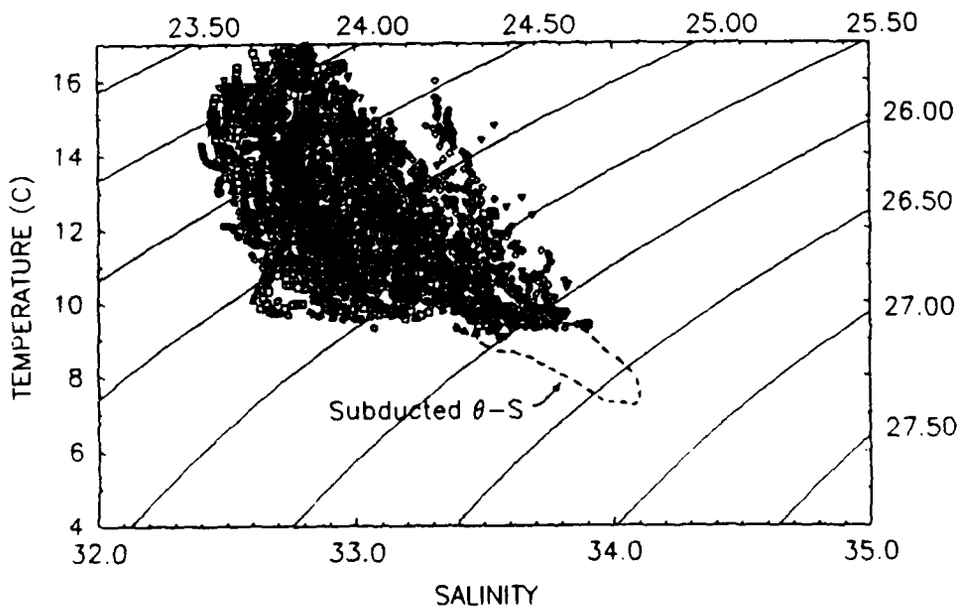
23.50
24.00
24.50
25.00
25.50
16
14
12
10
8
6
4
TEMPERATURE (C)
26.00
26.50
27.00
27.50
Subducted θ–S
32.0
33.0
34.0
35.0
SALINITY

C.

FIG. 9

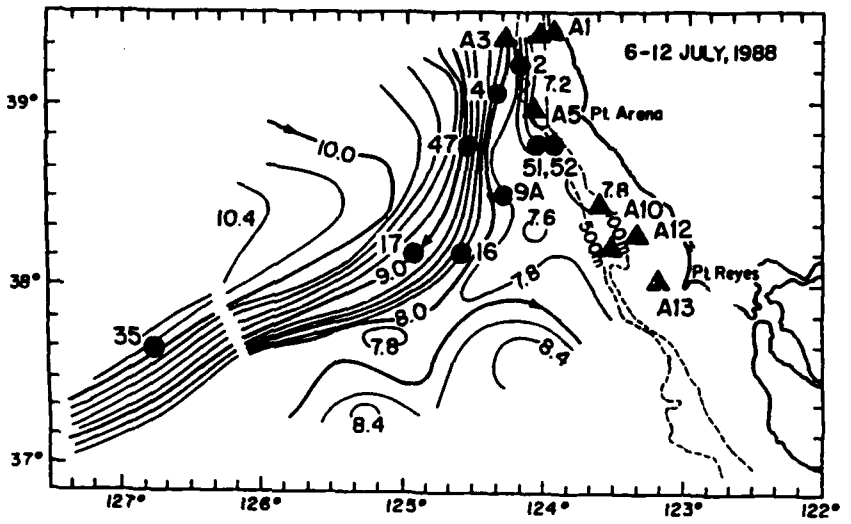
6-12 JULY, 1988
A1
A3
2
4
7.2
A5
Pt Arena
47
10.0
51,52
9A
7.8
A10
A12
10.4
7.6
17
16
9.0
1.8
Pt Reyes
A13
35
8.0
7.8
8.4
8.4
39°
38°
37°
127°
126°
125°
124°
123°
122°

A.

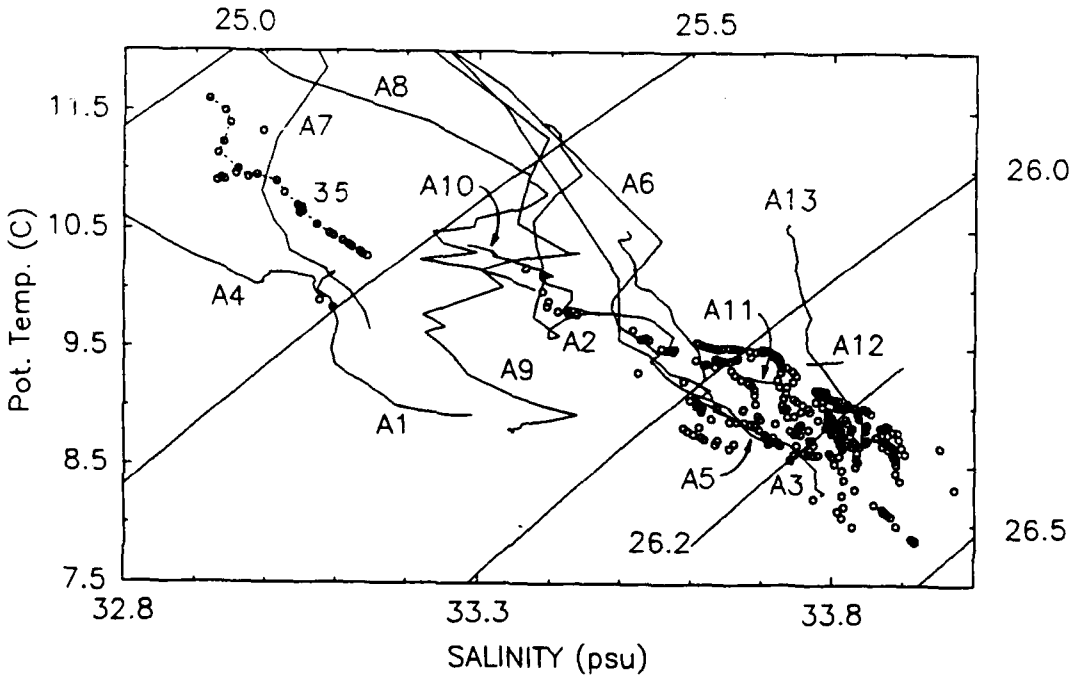
25.0
25.5
A8
A7
A10
A6
A13
35
A4
A2
A11
A12
A9
A1
A5
A3
26.2
26.0
26.5
11.5
10.5
9.5
8.5
7.5
Pot. Temp. (C)
32.8
33.3
33.8
SALINITY (psu)

B.

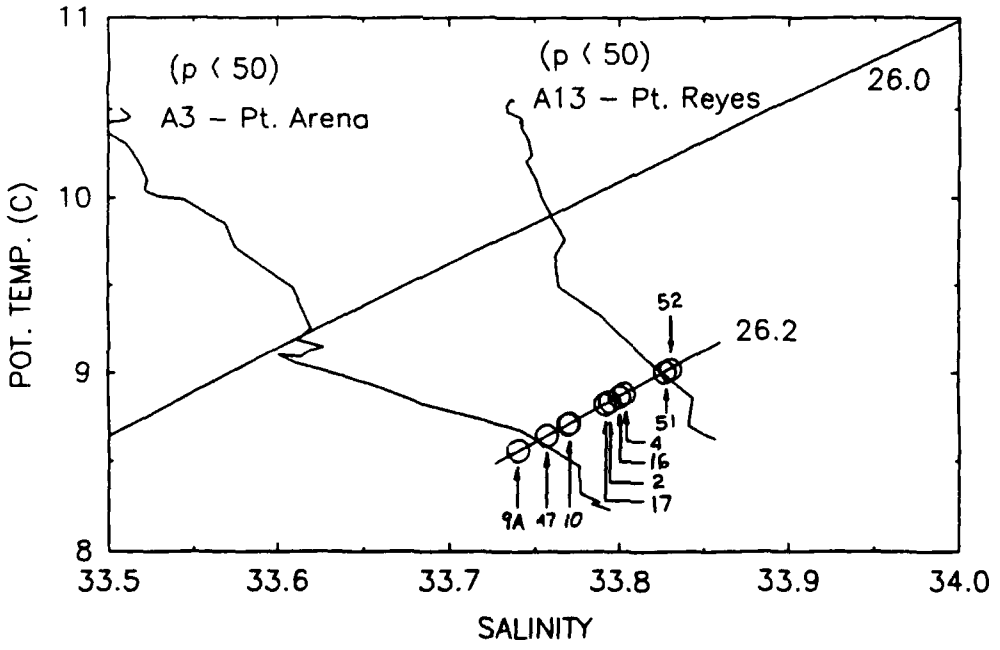
(p < 50)
A3 – Pt. Arena
(p < 50)
A13 – Pt. Reyes
26.0
52
26.2
51
4
16
2
17
9A
47
10
11
10
9
8
POT. TEMP. (C)
33.5
33.6
33.7
33.8
33.9
34.0
SALINITY

C.

FIG. 10

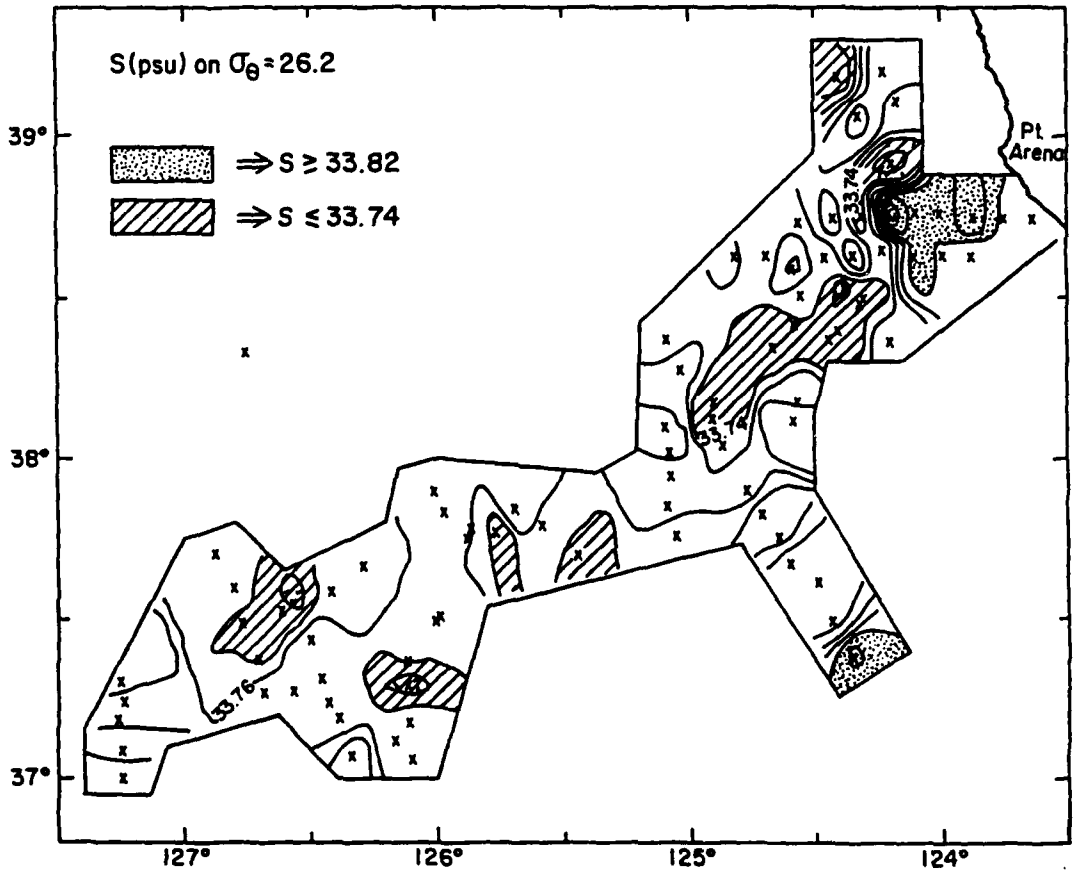
S(psu) on σ_θ = 26.2
⇒ S ≥ 33.82
⇒ S ≤ 33.74
39°
38°
37°
127°
126°
125°
124°
Pt. Arena
33.74
33.74
33.76

FIG. 11

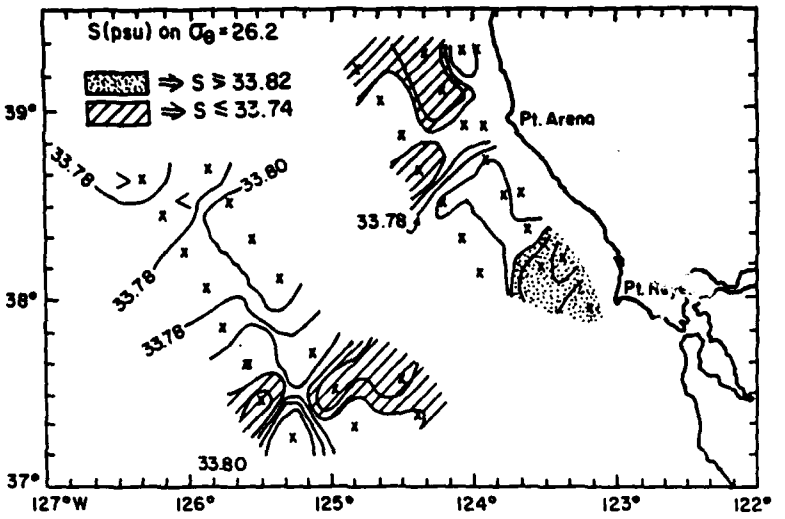
S(psu) on σ_θ=26.2
⇒ S ≥ 33.82
⇒ S ≤ 33.74
33.78
33.80
33.78
33.78
33.80
Pt. Arena
Pt. Reyes
39°
38°
37°
127°W
126°
125°
124°
123°
122°

A.

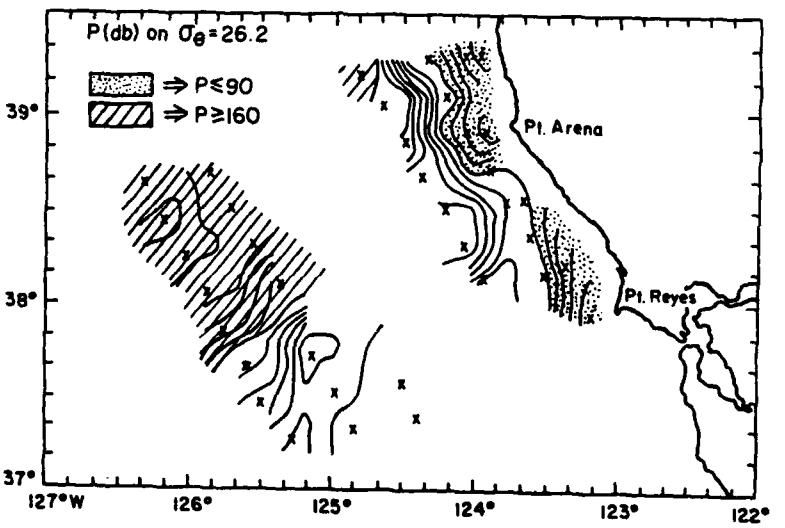
P(db) on σ_θ=26.2
⇒ P≤90
⇒ P≥160
Pt. Arena
Pt. Reyes
39°
38°
37°
127°W
126°
125°
124°
123°
122°

B.

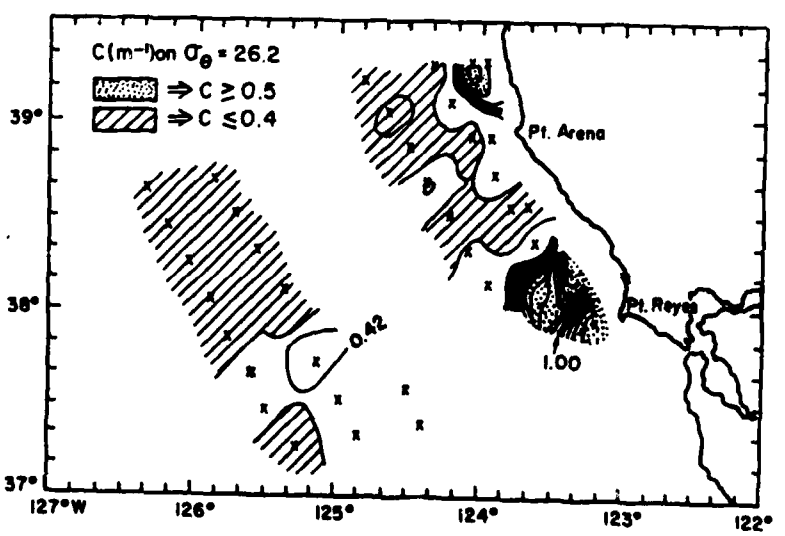
C(m⁻¹)on σ_θ = 26.2
⇒ C ≥ 0.5
⇒ C ≤ 0.4
0.42
1.00
Pt. Arena
Pt. Reyes
39°
38°
37°
127°W
126°
125°
124°
123°
122°

C.

FIG. 12

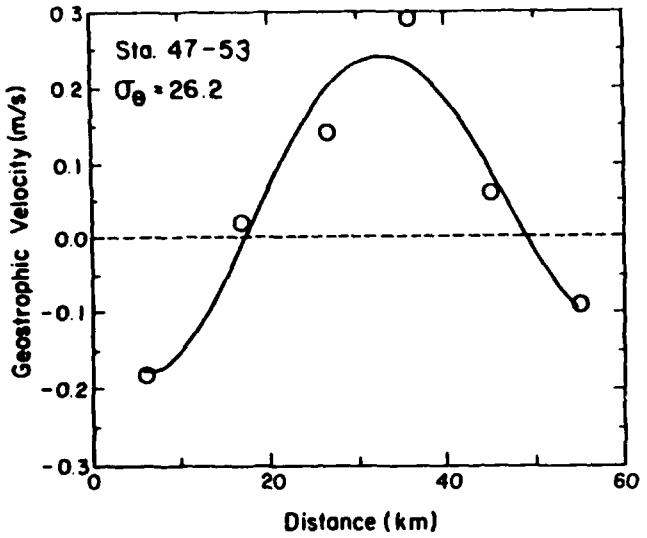
B.
Sta. 47-53
σ_θ = 26.2
Geostrophic Velocity (m/s)
Distance (km)

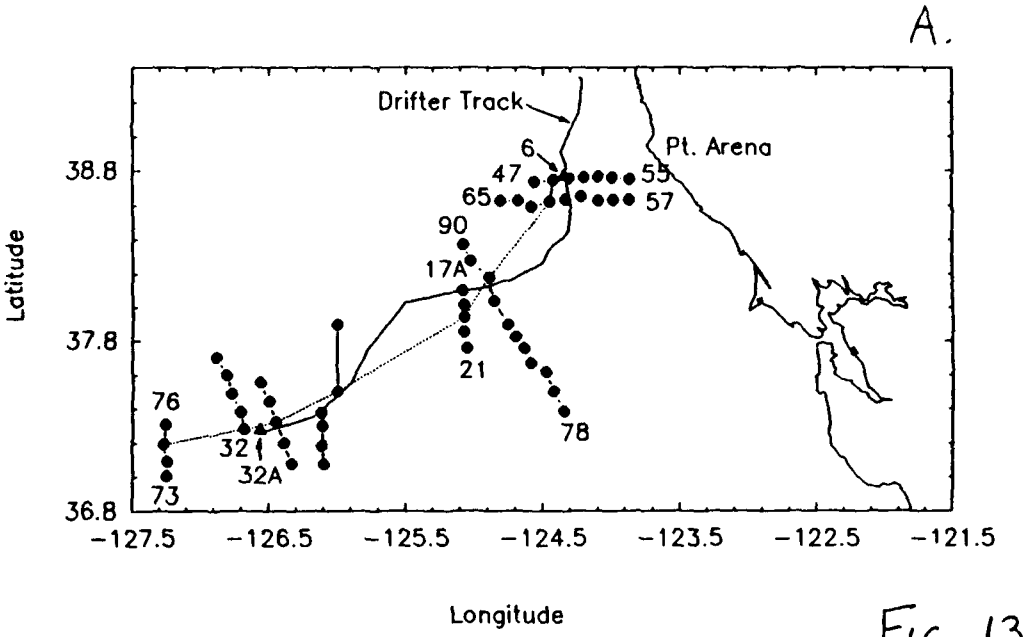
A.
Drifter Track
Pt. Arena
6
47
55
65
57
90
17A
21
76
32
32A
73
78
Latitude
Longitude

FIG. 13

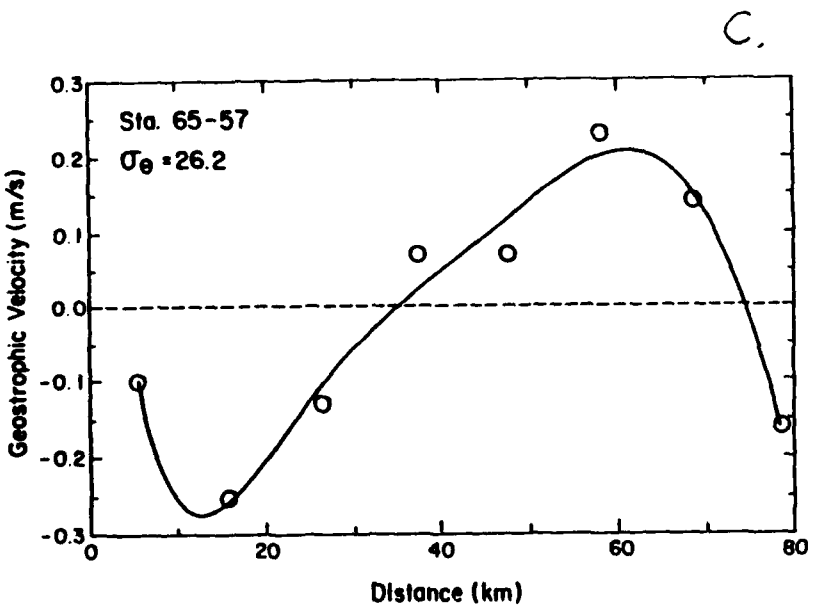
C.
Sta. 65-57
σ_θ = 26.2
Geostrophic Velocity (m/s)
Distance (km)

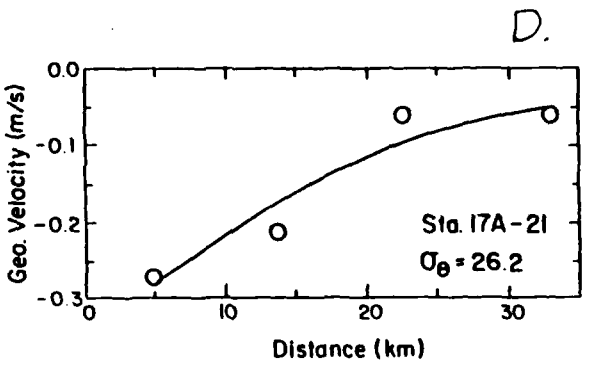
D.
Sta. 17A-21
σ_θ = 26.2
Geo. Velocity (m/s)
Distance (km)

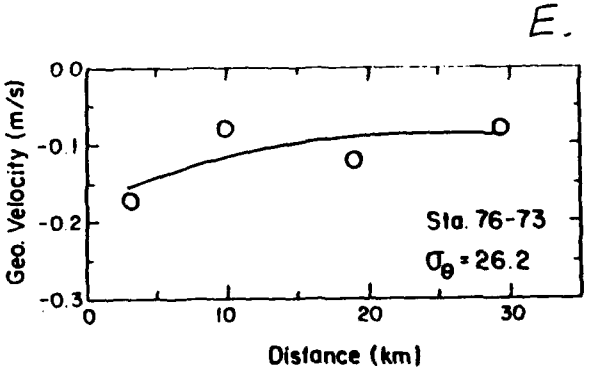
E.
Sta. 76-73
σ_θ = 26.2
Geo. Velocity (m/s)
Distance (km)

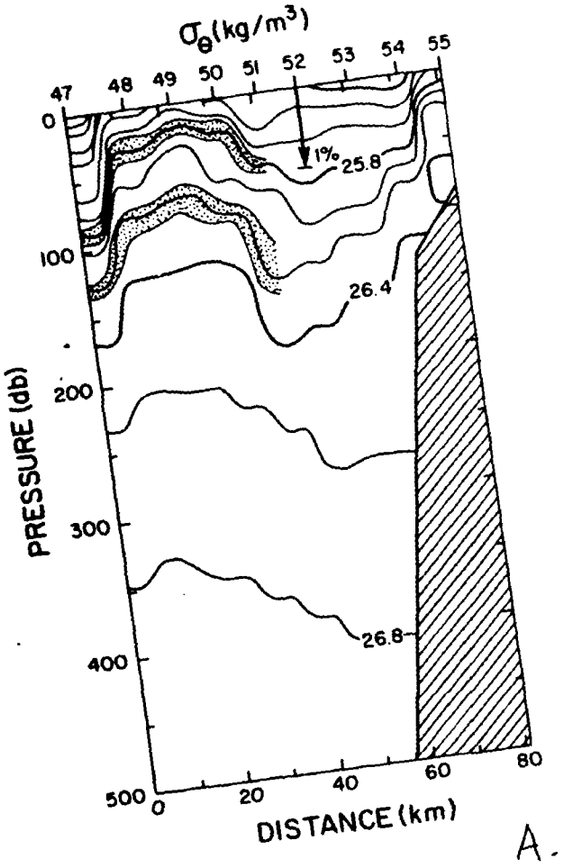
σ_θ(kg/m^3)
47 48 49 50 51 52 53 54 55
0
100
200
300
400
500
1%
25.8
26.4
26.8
PRESSURE (db)
0 20 40 60 80
DISTANCE (km)

A.

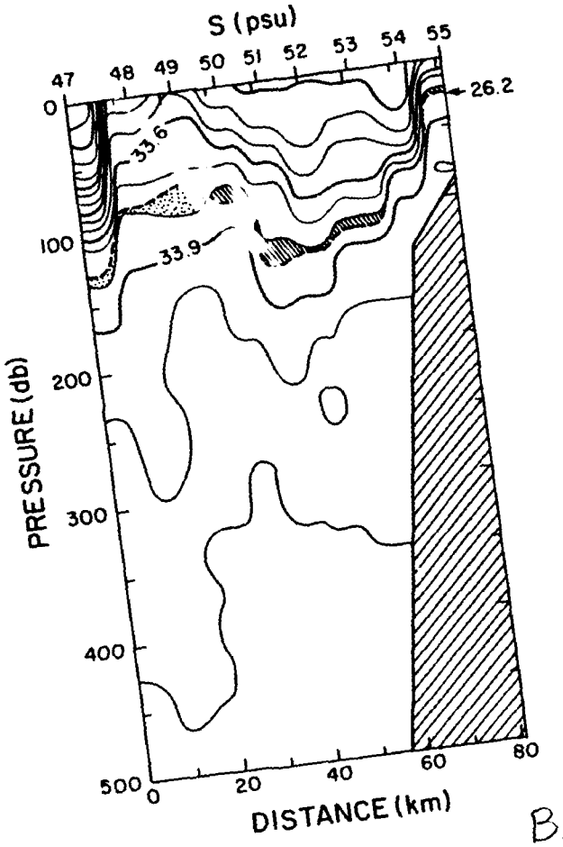
S (psu)
47 48 49 50 51 52 53 54 55
0
100
200
300
400
500
26.2
33.6
33.9
PRESSURE (db)
0 20 40 60 80
DISTANCE (km)

B.

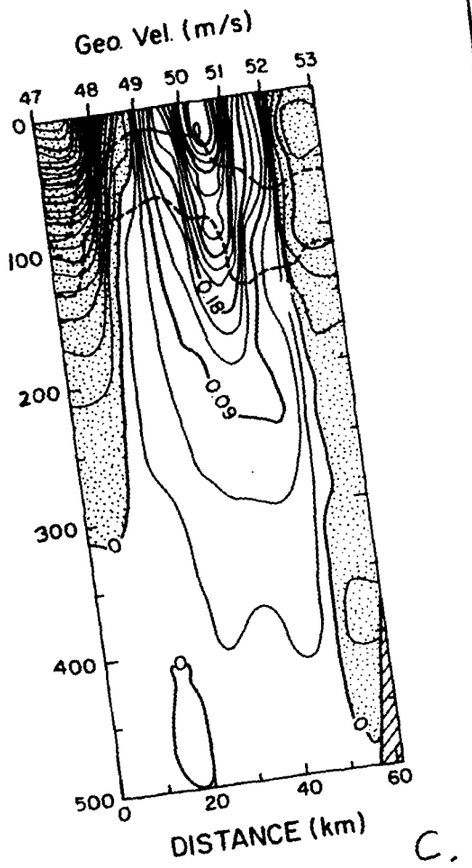
Geo. Vel. (m/s)
47 48 49 50 51 52 53
0
100
200
300
400
500
0.18
0.09
0
0
0
0 20 40 60
DISTANCE (km)

C.

FIG. 14

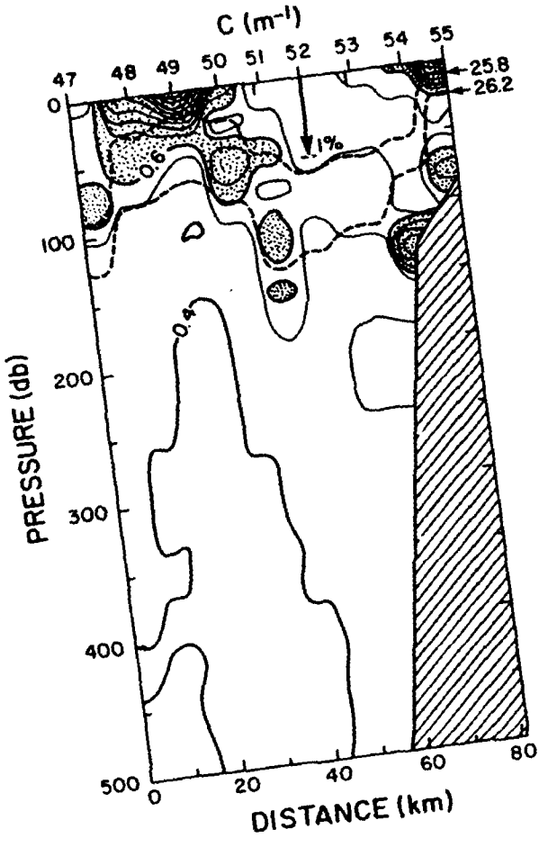
C (m⁻¹)
47 48 49 50 51 52 53 54 55
0
25.8
26.2
1%
0.6
0.4
100
200
300
400
500
PRESSURE (db)
0 20 40 60 80
DISTANCE (km)

D.

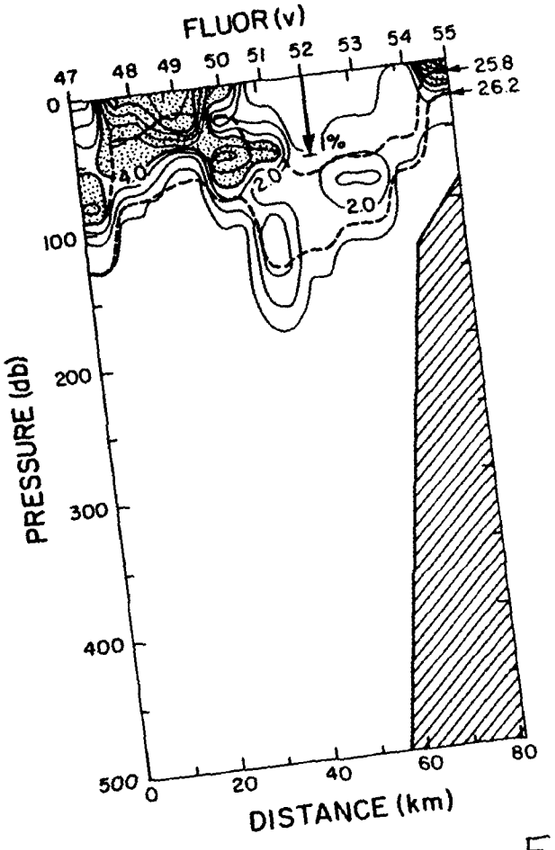
FLUOR (v)
47 48 49 50 51 52 53 54 55
0
25.8
26.2
1%
4.0
2.0
2.0
100
200
300
400
500
PRESSURE (db)
0 20 40 60 80
DISTANCE (km)

E.

FIG. 14

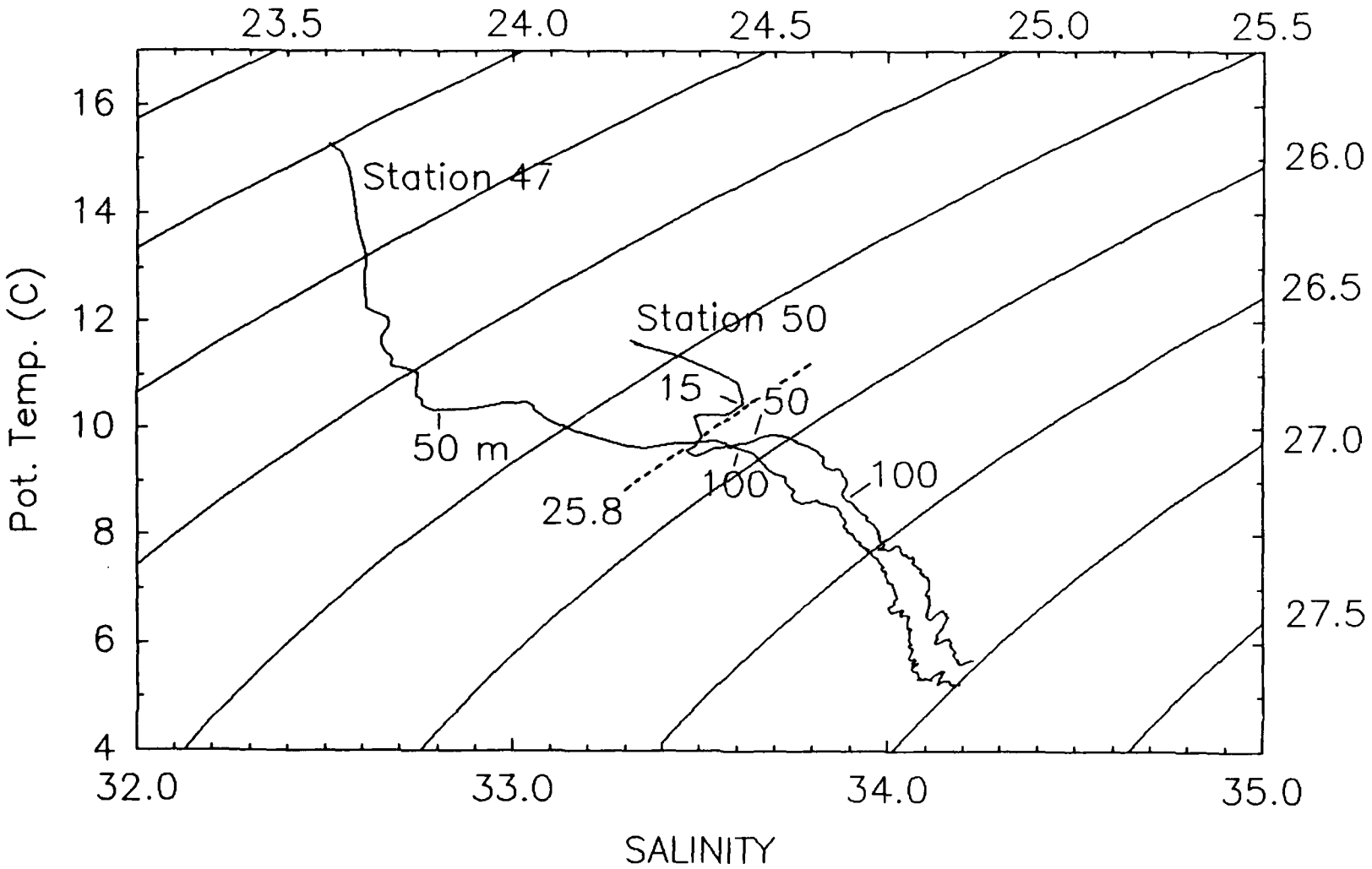
23.5
24.0
24.5
25.0
25.5
16
14
12
10
8
6
4
Pot. Temp. (C)
26.0
26.5
27.0
27.5
Station 47
Station 50
15
50
100
100
50 m
25.8
32.0
33.0
34.0
35.0
SALINITY

FIG. 15

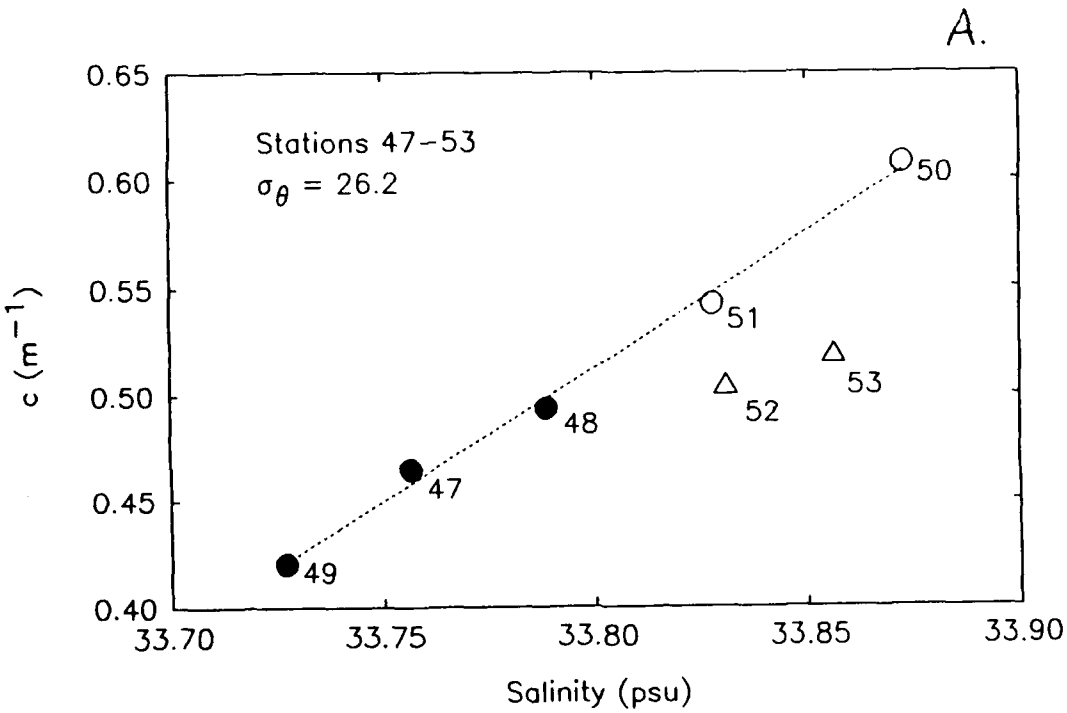
A.
Stations 47–53
σ_θ = 26.2
c (m^{-1})
0.65
0.60
0.55
0.50
0.45
0.40
33.70
33.75
33.80
33.85
33.90
Salinity (psu)
49
47
48
50
51
52
53

FIG. 16

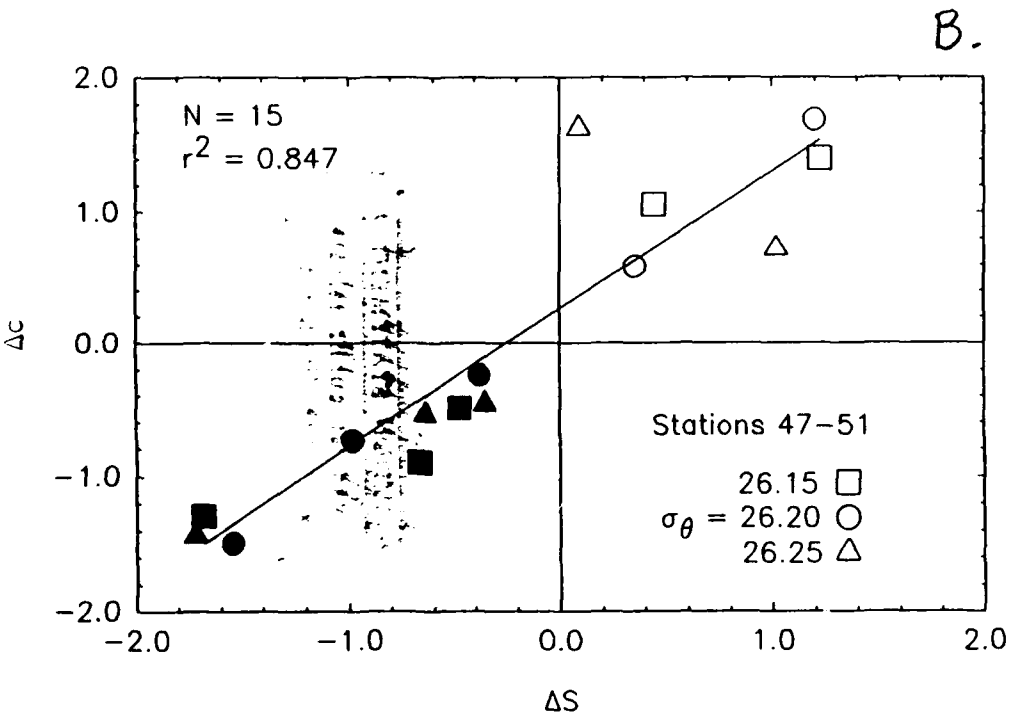
B.
N = 15
r^2 = 0.847
Stations 47–51
26.15
σ_θ = 26.20
26.25
Δc
ΔS
2.0
1.0
0.0
−1.0
−2.0
−2.0
−1.0
0.0
1.0
2.0

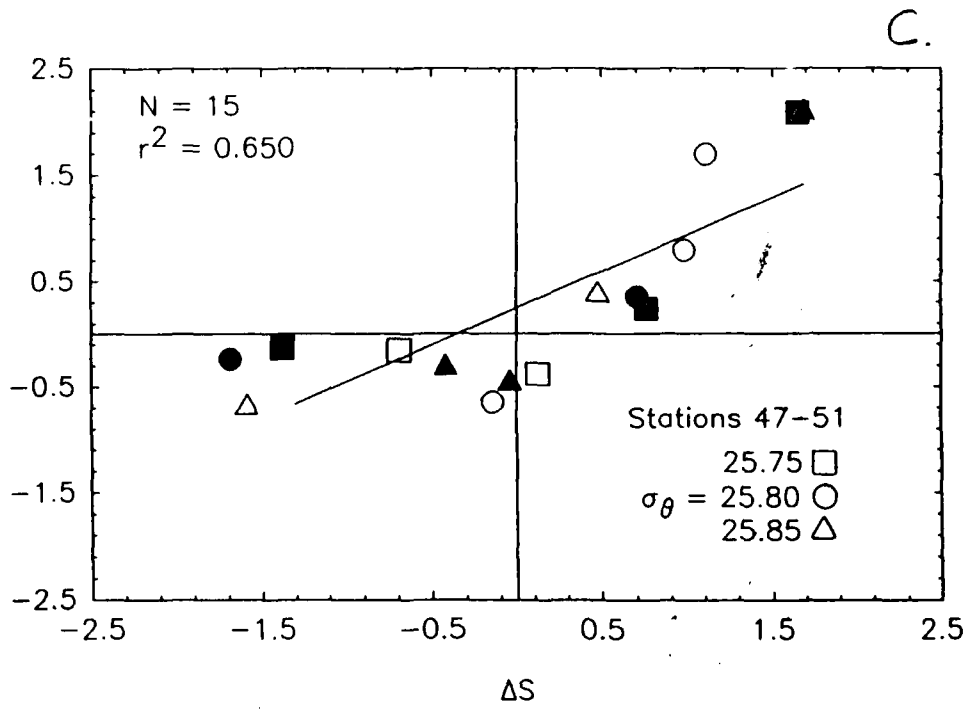
C.
N = 15
r^2 = 0.650
Stations 47–51
25.75
σ_θ = 25.80
25.85
ΔS
2.5
1.5
0.5
−0.5
−1.5
−2.5
−2.5
−1.5
−0.5
0.5
1.5
2.5